Modeling of Modulus Graded Axisymmetric Adhesive Joints

S Kumar [a], J P Scanlan [b]

[a] *Department of Materials Engineering, University of California, Santa Barbara,CA 93106, USA*

[b] *Computational Engineering and Design Centre, School of Engineering Sciences, University of Southampton, Southampton, SO17 1BJ, UK*

Abstract

This study presents a refined theoretical framework for the stress analysis of modulus graded axisymmetric adhesive joints which takes into account the radial stresses ($\sigma_{rr}^{(i)}$) in the bonded assembly. This semi-analytical is based on a variational method which minimizes the complementary energy of the bonded system. The joint consists of similar or dissimilar polar anisotropic composite adherends or metallic adherends and a functionally modulus graded bondline (FMGB) adhesive. The elastic modulus of the adhesive is functionally graded along the bondlength by assuming smooth modulus profiles which reflect the behavior of practically producible graded bondline. The stress distribution predicted by this refined model is compared with that of MMB model which also accounts for ($\sigma_{rr}^{(i)}$) in the bonded system to estimate reduction in shear and peel stress peaks in the bondline. The axisymmetric stress analysis reveals that the peel and shear stress peaks in the FMGB are much smaller and the stress distribution is more uniform along its length than those of mono-modulus bondline (MMB) adhesive joints under the same axial tensile load. A systematic parametric study has been conducted by selectively perturbing the material and geometrical properties of the joint in order to study their influence on stress distribution in the bondline. Furthermore, the results suggest that the peel and shear strengths can be optimized by spatially controlling the modulus of the adhesive.

Key words: Functionally modulus graded bondline, Adhesive joint, Stress concentration, Stress analysis, Variational method

1 Nomenclature

E_1, ν_1 Young's modulus and Poison's ratio of an isotropic inner adherend respectively
E_2, ν_2 Young's modulus and Poison's ratio of an isotropic outer adherend respectively
E, ν Young's modulus and Poison's ratio of the MMB adhesive
E_l^i, E_t^i, ν_{tl}^i, ν_{tt}^i, G_{tl}^i Elastic properties of polar anisotropic adherends (i=1 for inner adherend and i=2 for outer adherend)
E_{f1}, E_{f2}, E_{f3}, E_{f4}, E_{f5} Modulus functions of the FMGB Adhesive
E_m, E_o Maximum and minimum value of Young's modulus of the FMGB adhesive respectively
$E(z)$ Generic modulus function of the FMGB adhesive
a, b Inner and outer radii of the inner adherend respectively
c, d Inner and outer radii of the outer adherend respectively
t_1, t_2 Thickness of inner and outer adherends respectively
t Thickness of the adhesive layer
P Axial tensile load
L Bond length of the joint
r, θ, z Radial, circumferential and axial coordinates of the tubular system respectively
q, f Axial edge stresses in the inner and outer adherends of the jointed portion respectively
$\sigma_{rr}^{(i)}, \sigma_{\theta\theta}^{(i)}, \sigma_{zz}^{(i)}, \tau_{rz}^{(i)}$ Stress components in the bonded assembly (i=1 for inner adherend, i=2 for outer adherend and i=a for adhesive)
$\varepsilon_{rr}^{(i)}, \varepsilon_{\theta\theta}^{(i)}, \varepsilon_{zz}^{(i)}, \gamma_{rz}^{(i)}$ Elastic stress components in the bonded assembly (i=1 for inner adherend, i=2 for outer adherend and i=a for adhesive)
Π_1, Π_2, Π_3 Complementary energy in the inner adherend, outer adherend and adhesive respectively
Π Complementary energy of the bonded system

2 Introduction

Adhesively bonded joints are widely used in variety of industries for joining dissimilar materials since they provide more uniform load transfer over the bonded area. Weight reduction and improved fatigue life are the drivers for the extensive use of adhesively bonded joints. Numerous studies have been devoted to the stress analysis of bonded joints, both analytically and numerically, forming the basis for design and durability assessment of joints [1–14,45,51,52].

There are several types of tubular lap joints such as single lap joint, double

lap joint, stepped lap joint, scarf lap joint etc. Out of these, the tubular single lap joint is the most occurring one due to its ease of manufacture and its low cost. Initially, Lubkin and Reissner [1] analyzed the stress distribution in the adhesive of tubular lap joints composed of thin-walled circular cylindrical shell elements subjected to axisymmetric loading with the assumptions that the adhesive is thin and much more flexible than the adherends. They treated the adhesive as a series of infinitesimal coil springs. Later, the same problem was verified using axisymmetric quadratic isoparametric finite elements by Adams and Peppiatt [8]. Adams and Peppiatt also analyzed tubular lap joints under torsional loads.

A few researchers have proposed two-dimensional analytical solutions for cylindrical bonded joints, which were focused on the joint overlap, ensuring the stress free boundary conditions at the free ends. For instance, Allman [15] used a minimum strain energy, with given bending, stretching and shearing at the end of the overlap and assuming that the longitudinal normal stress was zero, the shear stress constant, and the transverse normal stress was linearly distributed across the thickness of the adhesive. Shi and Cheng [16] presented approximate closed form solutions for tubular bonded joints based on the variational principle of complementary energy with similar boundary conditions and assumptions to those of Allman. Lindon et al. [17] presented experimental and theoretical investigations to calculate strength of cylindrical assemblies with an anaerobic adhesive. Pugno and Carpinteri [18] analyzed static and dynamic behavior of tubular adhesive joints under axial load. Imanaka [19] proposed a method of fatigue strength estimation of adhesive bonded shaft joints based on experimental and finite element studies. Kumar and Pandey [47,46] recently evaluated fatigue performance of planar adhesive joints. Nayeb-Hashemi et al. [20] proposed a damage model for tubular joints under combined axial and torsional cyclic loading. Thomsen [21] carried out elasto-plastic numerical stress analysis of tubular lap joints comprising dissimilar orthotropic circular cylindrical laminated shells under non-axisymmetric type of loading and shown that the inelastic behavior of adhesive affects the adhesive stress distribution even at low levels of external loading. Kim et al. [22] included nonlinear properties and fabrication residual thermal stresses in the stress calculation of tubular single-lap carbon/epoxy composite-steel joints. Recently, Nemes et al. [23] provided a statically determinate elastic solution for the cylindrical lap-joint employing the same methodology as that of Shi and Cheng [16]. Kumar [49], Kumar and Scanlan [50] developed theoretical models for the stress analysis of cylindrical adhesive joints with modulus graded adhesive. In this current study, a refined semi-analytical model is presented for the stress analysis of tubular adhesive joints with a FMGB adhesive.

Several techniques have been used to minimize the stress concentrations at the ends of the overlap of single lap joints and hence to improve structural capability [24–26]. These include altering the adherend geometry [27–29], the

adhesive geometry [30] and the spew geometry [31,32]. These studies mostly focused on geometrical aspect of adhesive and adherends to minimize stress concentration. Nevertheless, in a few cases, change of geometry is limited by complexities involved in production besides the cost. A few researchers altered the material of the adhesive globally to achieve higher joint strength. They studied the effect of the shear modulus of adhesive on the shear stress distribution in the bondline and showed that it has a considerable effect [24,33]. Sadek [34] has shown that the lap-shear strength of the joints can be enhanced by introducing stiff adhesive in the bondline. However, in this case, adhesives are prone to interfacial brittle failure owing to high peel stresses they experience. Even if a complaint adhesive is employed in the bondline, the stress distribution in the bonded area would be non-uniform [34]. On the other hand, swapping the material of the adherends would not be possible because the adherend material is selected based on the functional requirement of the structural members to be bonded. However, the material properties of the adherends or adhesive can be altered in the overlap region. Ganesh et al. [35] showed that composite materials with continuously varying material properties can be fabricated by modifying the conventional braiding technology of fiber placement. Boss et al. [36] studied the stress distribution in the adhesive of a single-lap joint with modulus and geometrically graded composite adherend. Recently, Pires et al. [37,38] and Fitton and Broughton [39] have evaluated performance of bi-adhesive bonded lap joints and have shown considerable increase in joint strength compared to mono-adhesive joints. Temiz [40] numerically examined the bi-adhesive double-strap joints under bending moment. Kumar and Pandey [41] performed 2D and 3D FE studies on bi-adhesive single lap joints and shown that the 3D analysis is indispensable for the design of such joints. Da Silva and Adams [42] have shown that at high and low temperatures joints strength can be significantly improved if dissimilar adherends along with dual adhesives are employed. All these investigators have considered only one step variation in adhesive modulus over the bondlength. Therefore, in this current study, a multi-step variation of the modulus of the adhesive along its length has been considered so as to reduce peel and shear stress peaks and to minimise their non-uniform distribution in the bondline. The task is to formulate the adhesive and adherends stresses in terms of geometrical and mechanical properties of the shaft-tube assembly.

3 Axisymmetric model

It has been demonstrated by Kumar [49], Kumar and Scanlan [50] that the load carrying capacity of the adhesively bonded cylindrical joints subjected to axial tensile loads can be significantly improved by employing a functionally modulus graded bondline (FMGB) adhesive in lieu of a mono modulus

bondline (MMB) adhesive. In those models, authors intentionally omitted the radial stresses ($\sigma_{rr}^{(i)}$) in the bonded system in order to develop a simple theoretical framework which allows them to predict the stress distribution in the bonded system. In this present study, authors realistically consider the non-zero radial stresses ($\sigma_{rr}^{(i)} \neq 0$) in the bonded assembly and developed a more accurate model to determine the stress state in the bonded system while using an adhesive whose modulus vary along the bondlength of the joint.

Consider two hollow cylinders of different materials and dimensions as shown in Fig. 1a. The two cylinders are lap-jointed by a FMGB adhesive. The joint is subjected to an axial tensile load P. Fig. 1b shows the coordinate system with coordinates r and z and the edge stresses (q and f of the bonded portion whose length is L.

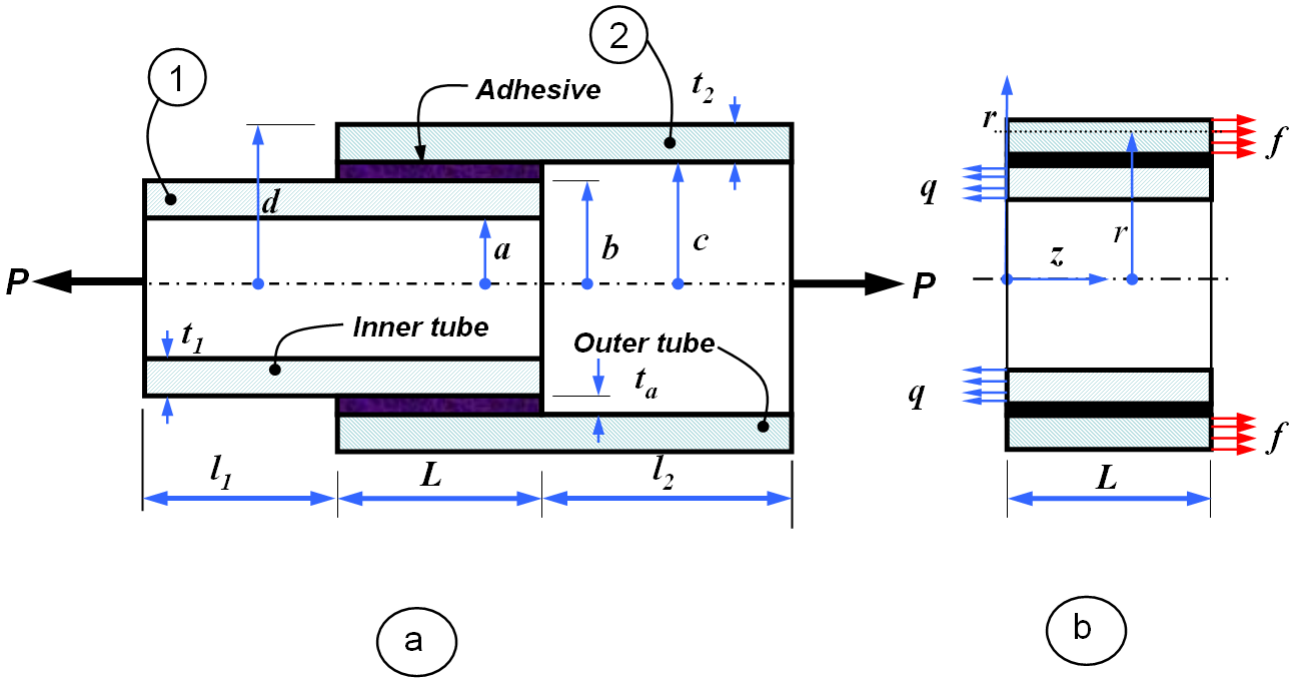

Fig. 1. a. Adhesively bonded tubular joint b. Coordinate system (r,θ,z) and edge stresses on jointed portion

The aim of the problem is to determine the stress distribution in the adhesive layer when using an adhesive where properties vary along the length of the joint.

The following assumptions have been adopted to analyze this statically determinate system.

- The radial stress in the inner and outer adherends is a function of the radius r only. i.e. $\sigma_{rr}^{(1)} = \sigma_{zz}^{(1)}(r); \sigma_{rr}^{(2)} = \sigma_{rr}^{(2)}(r)$ and the radial stress in the adhesive is constant i.e. $\sigma_{rr}^{(a)} = \chi$

- Axisymmetric condition implies that the following shear stresses are zero i.e $\tau_{r\theta}^{(i)} = 0, \tau_{z\theta}^{(i)} = 0$ in all three domains.
- For a thin adhesive, the difference between the two shearing stresses acting on the outer surface of the adhesive $\tau_{rz}^{(a)}(c,z)$ and that on the inner surface of the adhesive $\tau_{rz}^{(a)}(b,z)$ is very small and, hence, the longitudinal stress $\sigma_{zz}^{(a)}$ in the adhesive may be neglected as compared with shearing stress $\tau_{rz}^{(a)}$.
- The longitudinal stress in the inner and outer adherends is a function of the axial coordinate z only. i.e. $\sigma_{zz}^{(1)} = \sigma_{zz}^{(1)}(z); \sigma_{zz}^{(2)} = \sigma_{zz}^{(2)}(z)$

Therefore, the non-zero stress components in the bonded system are:

- Inner adherend: $\sigma_{rr}^{(1)}(r)$, $\tau_{rz}^{(1)}(r,z), \sigma_{\theta\theta}^{(1)}(r,z), \sigma_{zz}^{(1)}(z)$
- Adhesive: $\sigma_{rr}^{(a)}$, $\tau_{rz}^{(a)}(r,z), \sigma_{\theta\theta}^{(a)}(r,z)$
- Outer adherend: $\sigma_{rr}^{(2)}(r)$, $\tau_{rz}^{(2)}(r,z), \sigma_{\theta\theta}^{(2)}(r,z), \sigma_{zz}^{(2)}(z)$

Incorporating the aforementioned assumptions, the differential equations of equilibrium are reduced to the following.

$$\frac{1}{r}\frac{\partial}{\partial r}(r\sigma_{rr}^{(i)}) + \frac{\partial \tau_{rz}^{(i)}}{\partial z} - \frac{\sigma_{\theta\theta}^{(i)}}{r} = 0 \tag{1}$$

$$\frac{1}{r}\frac{\partial}{\partial r}(r\tau_{rz}^{(i)}) + \frac{\partial \sigma_{zz}^{(i)}}{\partial z} = 0 \tag{2}$$

The stress field in the axisymmetric system should satisfy the equations of equilibrium, the traction boundary conditions prescribed at $z = 0; z = L$, and the conditions of stress continuity across the dividing surfaces ($r = b; r = c$). The equilibrium of the bonded system gives the following relationship between q and f

$$q(b^2 - a^2) = f(d^2 - c^2) = \sigma_{zz}^{(1)}(b^2 - a^2) + \sigma_{zz}^{(2)}(d^2 - c^2) + \sigma_{zz}^{(a)}(c^2 - b^2) \tag{3}$$

Noting that the longitudinal stress in the adhesive, $\sigma_{zz}^{(a)}$ is zero, the longitudinal stress in outer adherend is given by

$$\sigma_{zz}^{(2)} = f + \rho\, \sigma_{zz}^{(1)} \tag{4}$$

where,

$$\rho = \frac{(b^2 - a^2)}{(c^2 - d^2)} \tag{5}$$

3.1 Stress fields in the adherends and adhesive

In this refined model, the radial stresses in the adherends ($\sigma_{rr}^{(i)}$, i=1 for inner adherend, i=2 for outer adherend) are assumed to vary as a nonlinear function of the radius r, while the radial stress in the adhesive ($\sigma_{rr}^{(a)}$) is assumed to be constant across the thickness of adhesive layer as shown in Fig. 2.

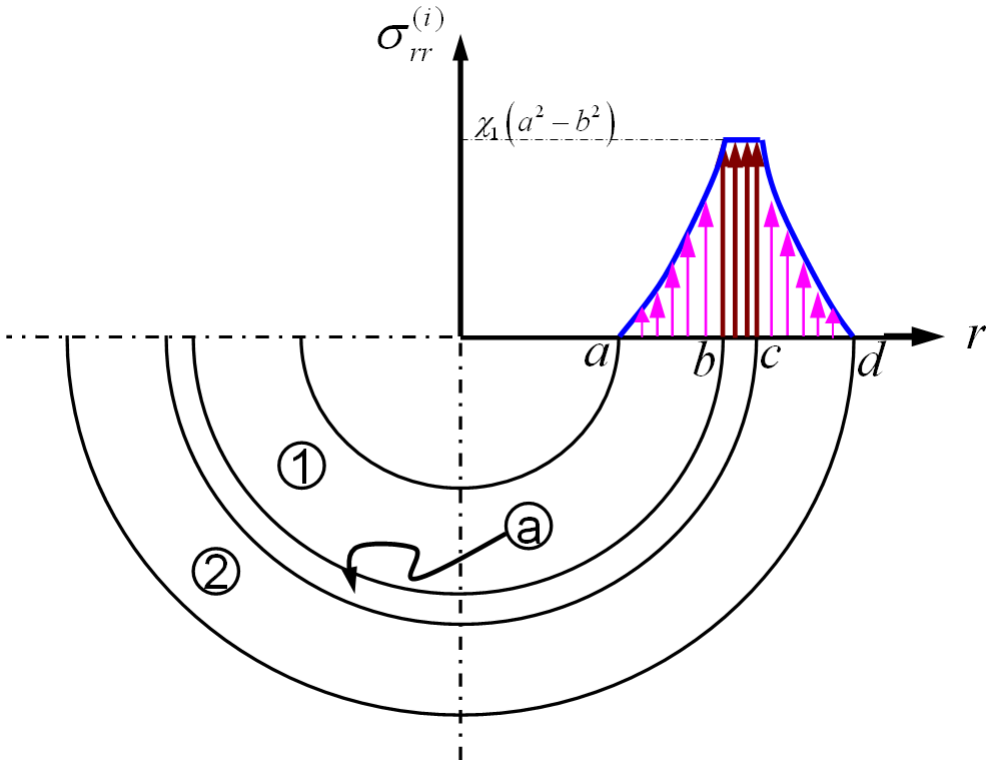

Fig. 2. Variation of radial stress across the radius of the bonded system: 1,2: adherends and a: adhesive

3.1.1 Inner adherend

The radial stress in the inner adherend is given by

$$\sigma_{rr}^{(1)} = \chi_1\left(a^2 - r^2\right) \tag{6}$$

where, χ_1 is a constant. χ_1 depends upon material and geometrical properties as well as loading condition of the joint. Considering equilibrium of an elemental length dz of the inner tube as shown in Fig. 3a, the shear stress $\tau_{rz}^{(1)}$ is given by

$$\tau_{rz}^{(1)}(r,z) = \frac{(r^2-a^2)}{2r}\frac{d\sigma_{zz}^{(1)}}{dz} \tag{7}$$

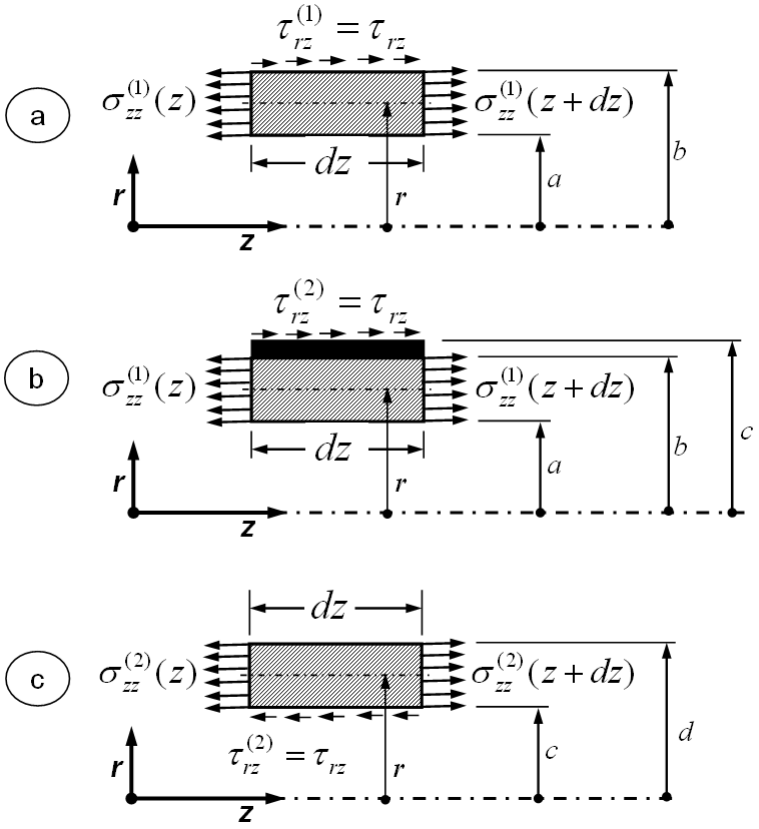

Fig. 3. a. Equilibrium of the inner tube b. Equilibrium of the inner tube and adhesive c. Equilibrium of the outer tube

Using $\tau_{rz}^{(1)}$ given by eqn. 7 and $\sigma_{rr}^{(1)}$ given by eqn. 6 in the equilibrium eqn. 1, we can get the tangential stress in the inner adherend and is given by

$$\sigma_{\theta\theta}^{(1)}(r,z) \;=\; \chi_1\left(a^2 - 3r^2\right) + \frac{(r^2-a^2)}{2}\frac{d^2\sigma_{zz}^{(1)}}{dz^2} \tag{8}$$

3.1.2 Adhesive

The radial stress in the adhesive is assumed to be constant across the thickness of the adhesive as it is very thin compared to adherends and is given by

$$\sigma_{rr}^{(a)} \;=\; \chi \tag{9}$$

here, χ is another constant. Similarly considering equilibrium of the elemental length dz of the inner adherend and adhesive together as depicted in Fig. 3b, we can express $\tau_{rz}^{(a)}$ as

$$\tau_{rz}^{(a)}(r,z) \;=\; \frac{(b^2-a^2)}{2r}\frac{d\sigma_{zz}^{(1)}}{dz} \tag{10}$$

Again, using expressions for $\tau_{rz}^{(a)}$ and $\sigma_{rr}^{(a)}$ in the equilibrium eqn. 1, the circumferential stress $\sigma_{\theta\theta}^{(a)}$ in the adhesive is obtained as

$$\sigma_{\theta\theta}^{(a)}(r,z) \;=\; \chi_1\left(a^2-b^2\right)+\frac{(b^2-a^2)}{2}\frac{d^2\sigma_{zz}^{(1)}}{dz^2} \tag{11}$$

Note that the circumferential stress in the adhesive is independent of r since we assumed that σ_{zz} is negligible.

3.1.3 Outer adherend

The radial stress in the outer adherend $\sigma_{rr}^{(2)}$ varies nonlinearly with r (see Fig. 2) and is given by

$$\sigma_{rr}^{(2)} \;=\; \chi_2\left(d^2-r^2\right) \tag{12}$$

χ_2 is yet another constant. To ensure the continuity of radial stress at the interfaces ($r=b, r=c$), the following condition needs to be satisfied.

$$\chi \;=\; \chi_1\left(a^2-b^2\right)=\chi_2\left(d^2-c^2\right) \tag{13}$$

Therefore χ_2 is given by

$$\chi_2 \;=\; \chi_1\,\rho \tag{14}$$

Considering equilibrium of elemental length dz of the outer adherend as shown in Fig. 3c, the shear stress is given as a function of the gradient of longitudinal stress in the outer adherend

$$\tau_{rz}^{(2)}(r,z) \;=\; \frac{(r^2-d^2)}{2r}\frac{d\sigma_{zz}^{(2)}}{dz} \tag{15}$$

Applying the shear stress continuity condition at the adhesive-adherend outer interface ($\tau_{rz}^{(2)}$ at $r=c$ is equal to $\tau_{rz}^{(a)}$ at $r=c$), we can relate the longitudinal stress gradients of both adherends

$$\frac{d\sigma_{zz}^{(2)}}{dz} \;=\; \frac{(b^2-a^2)}{(c^2-d^2)}\frac{d\sigma_{zz}^{(1)}}{dz}=\rho\;\frac{d\sigma_{zz}^{(1)}}{dz} \tag{16}$$

Using the above in eqn. 15, we get,

$$\tau_{rz}^{(2)}(r,z) \;=\; \rho\;\frac{(r^2-d^2)}{2r}\frac{d\sigma_{zz}^{(1)}}{dz} \tag{17}$$

Now, using expressions for $\sigma_{rr}^{(2)}$, χ_2 and $\tau_{rz}^{(2)}(r,z)$ in equilibrium eqn. 1

$$\sigma_{\theta\theta}^{(2)}(r,z) \;=\; \rho\;\chi_1\left(d^2-3r^2\right)+\;\rho\;\frac{(r^2-d^2)}{2}\frac{d^2\sigma_{zz}^{(1)}}{dz^2} \tag{18}$$

It is clear from the above mentioned equations that the radial, shear and the peel stresses are continuous across the adherend-adhesive interfaces. Thus, the stress components in the inner adherend $(\sigma_{rr}^{(1)}(r), \tau_{rz}^{(1)}(r,z), \sigma_{\theta\theta}^{(1)}(r,z))$, in the adhesive $(\sigma_{rr}^{(a)}, \tau_{rz}^{(a)}(r,z), \sigma_{\theta\theta}^{(a)}(r,z))$ and in the outer adherend $(\sigma_{rr}^{(2)}(r)$, $\tau_{rz}^{(2)}(r,z)$, $\sigma_{\theta\theta}^{(2)}(r,z), \sigma_{zz}^{(2)}(z))$ are expressed in terms of a single unknown stress function $\sigma_{zz}^{(1)}(z)$. Now the statically determinate problem is solved applying the traction boundary conditions prescribed at the ends of overlap. The boundary conditions are:

$$\sigma_{zz}^{(1)}(0) \;= q\;; \qquad \sigma_{zz}^{(1)}(L) \;= 0\;; \tag{19}$$

$$\tau_{rz}^{(a)}(r,0) = 0\;; \qquad \tau_{rz}^{(a)}(r,L) = 0\;; \qquad r\in[b,c] \tag{20}$$

3.2 FMGB adhesive

A few researchers have considered a single step variation of bondline modulus and justified the studies as showing a better joint performance. In this work, the bondline adhesive considered has a multi-step variation of modulus along the bondlength as shown in Fig. 4. The multi-step variation of modulus in the tubular joint can be obtained by applying a number of rings of adhesive of different moduli in the bondline. The stiff ones are applied in the middle portion of the bondline while the flexible ones are applied at the overlap end zones. As the lengths of individual slices tend to zero, the multi-modulus bondline exactly represents the smoothly varying modulus function. The smoothly varying modulus function given by E_{f2} is shown in Fig. 4 The modulus function is approximated such that

$$\int_0^L E_f(z)dz \;\approx\; 2E_0L_0 + 2E_1L_1 + \ldots\ldots\ldots\ldots\ldots + 2E_{m-1}L_{m-1} + E_mL_m \tag{21}$$

The various modulus profiles examined in the analysis are given below and are shown in Fig. 5 in normalized form. These modulus functions are arbitrarily chosen.

$$E_{f_1} \;=\; E_m\,\mathrm{e}^{-4\,\ln\left(\frac{E_m}{E_o}\right)\left(\frac{z}{L}-\frac{1}{2}\right)^2} \tag{22}$$

$$E_{f_2} \;=\; 4\;(E_o-E_m)\left(\frac{z^2}{L^2}-\frac{z}{L}\right)+E_o \tag{23}$$

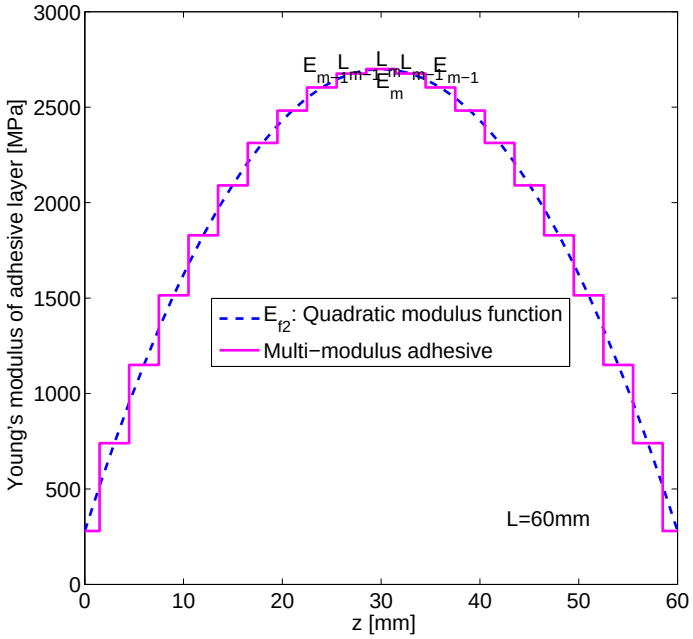

Fig. 4. Representation of multi-modulus bondline as a functionally modulus graded bondline

$$E_{f_3} = 8\,(E_m - E_o)\left(2\left(\frac{z}{L}-\frac{1}{2}\right)^4 - \left(\frac{z}{L}-\frac{1}{2}\right)^2\right) + E_m \tag{24}$$

$$E_{f_4} = \frac{64}{5}\,(E_o - E_m)\left(\left(\frac{z}{L}-\frac{1}{2}\right)^6 + \left(\frac{z}{L}-\frac{1}{2}\right)^4\right) + E_m \tag{25}$$

$$E_{f_5} = E_m \tag{26}$$

4 Constitutive models of the adherends and FMGB adhesive

The polar anisotropic constitutive relationship of the adherends is given below. Here i=1 for inner adhrend and i=2 for outer adhrend.

$$\begin{bmatrix} \sigma_{rr}^{(i)} \\ \sigma_{\theta\theta}^{(i)} \\ \sigma_{zz}^{(i)} \\ \tau_{rz}^{(i)} \end{bmatrix} = \begin{bmatrix} \frac{E_t^i}{1-\nu_{lt}^i\,\nu_{tl}^i} & \frac{\nu_{tt}^i\,E_t^i}{1-{\nu_{tt}^i}^2} & \nu_{lt}^i\,E_t^i & 0 \\ \frac{\nu_{tt}^i\,E_t^i}{1-{\nu_{tt}^i}^2} & \frac{E_t^i}{1-\nu_{lt}^i\,\nu_{tl}^i} & \nu_{lt}^i\,E_t^i & 0 \\ \nu_{lt}^i\,E_t^i & \nu_{lt}^i\,E_t^i & \frac{E_l^i}{1-\nu_{lt}^i\,\nu_{tl}^i} & 0 \\ 0 & 0 & 0 & G_{tl}^i \end{bmatrix} \begin{bmatrix} \varepsilon_{rr}^{(i)} \\ \varepsilon_{\theta\theta}^{(i)} \\ \varepsilon_{zz}^{(i)} \\ \gamma_{rz}^{(i)} \end{bmatrix}$$

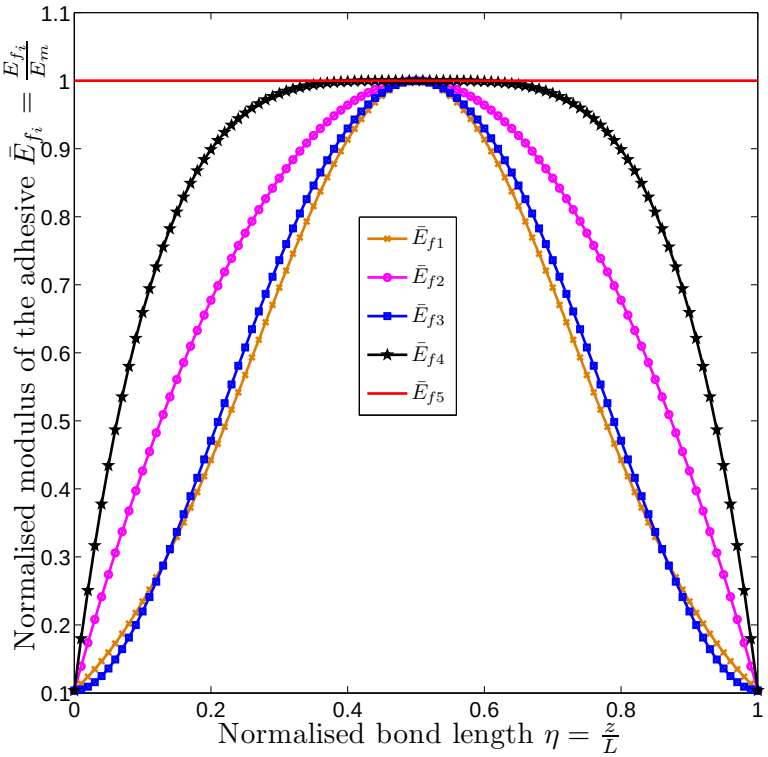

Fig. 5. Variation of Young's modulus of the adhesive over the bond length

Also $\nu^i_{lt}E^i_l = \nu^i_{tl}E^i_t$. Note that there are there are five independent constants. For the FMGB adhesive the axisymmetric constitutive model is given by

$$\begin{bmatrix} \sigma^{(a)}_{rr} \\ \sigma^{(a)}_{\theta\theta} \\ \sigma^{(a)}_{zz} \\ \tau^{(a)}_{rz} \end{bmatrix} = \frac{E(z)}{(1+\nu)(1-2\nu)} \begin{bmatrix} 1-\nu & \nu & \nu & 0 \\ \nu & 1-\nu & \nu & 0 \\ \nu & \nu & 1-\nu & 0 \\ 0 & 0 & 0 & 1/2(1-\nu) \end{bmatrix} \begin{bmatrix} \varepsilon^{(a)}_{rr} \\ \varepsilon^{(a)}_{\theta\theta} \\ \varepsilon^{(a)}_{zz} \\ \gamma^{(a)}_{rz} \end{bmatrix}$$

5 Variational technique

The variational method can be based either on an assumed infinitesimal displacement field in conjunction with the principle of minimum potential energy or on an assumed small stress variation associated with the complementary energy theorem [43]. In the current work, the second route has been pursued, following the analysis developed by Shi and Cheng [16] for tubular-lap joints and extending it to bonded systems with a FMGB adhesive. The problem can

be defined as obtaining a solution for $\sigma_{zz}^{(1)}$ by minimizing the complementary energy of the bonded system where the stresses for the adherends and FMGB adhesive have been defined in terms of a single stress function $\sigma_{zz}^{(1)}$. The admissible stress states are those which satisfy continuum differential equations of equilibrium, stress boundary conditions, stress-free end conditions of the joint and stress continuity at the adherend-adhesive interfaces. Once $\sigma_{zz}^{(1)}$ has been obtained, then all the stress components in the adhesive can be obtained. A true lower bound solution can be obtained in this way.

5.1 Case I: FMGB1 ($\sigma_{rr}^{(i)} \neq 0, i.e \quad \chi_1 \neq 0$)

The complementary energy of the joint comprising polar anisotropic adherends and a functionally modulus graded adhesive is given by Π, where

$$\Pi \;=\; \Pi_1 + \Pi_2 + \Pi_3 \tag{27}$$

Π_1 is the complementary energy of the inner adherend, Π_2 is the complementary energy of the outer adherend and Π_3 is the complementary energy of the FMGB adhesive. Π_1, Π_2 and Π_3 are given by

$$\Pi_1 \;=\; \pi \int_0^L \int_a^b \left[\sigma_{rr}^{(1)}\varepsilon_{rr}^{(1)} + \sigma_{zz}^{(1)}\varepsilon_{zz}^{(1)} + \sigma_{\theta\theta}^{(1)}\varepsilon_{\theta\theta}^{(1)} + \tau_{rz}^{(1)}\gamma_{rz}^{(1)}\right] r\, dr\; dz \tag{28}$$

$$\Pi_2 \;=\; \pi \int_0^L \int_c^d \left[\sigma_{rr}^{(2)}\varepsilon_{rr}^{(2)} + \sigma_{zz}^{(2)}\varepsilon_{zz}^{(2)} + \sigma_{\theta\theta}^{(2)}\varepsilon_{\theta\theta}^{(2)} + \tau_{rz}^{(2)}\gamma_{rz}^{(2)}\right] r\, dr\; dz \tag{29}$$

$$\Pi_3 \;=\; \pi \int_0^L \int_b^c \left[\sigma_{rr}^{(a)}\varepsilon_{rr}^{(a)} + \sigma_{\theta\theta}^{(a)}\varepsilon_{\theta\theta}^{(a)} + \tau_{rz}^{(a)}\gamma_{rz}^{(a)}\right] r\, dr\; dz \tag{30}$$

Π_1 and Π_2 for polar anisotropic adherends can be evaluated by using the strains $(\varepsilon_{rr}^{(i)}, \varepsilon_{\theta\theta}^{(i)}, \varepsilon_{zz}^{(i)}, \gamma_{rz}^{(i)})$ given by the anisotropic constitutive model described earlier.

For an isotropic system, Π_1, Π_2 and Π_3 become

$$\Pi_1 = \frac{\pi}{E_1} \int_0^L \int_a^b \Big\{\sigma_{rr}^{(1)2} + \sigma_{zz}^{(1)2} + \sigma_{\theta\theta}^{(1)2} - 2\nu_1 \left(\sigma_{rr}^{(1)}\sigma_{zz}^{(1)} + \sigma_{rr}^{(1)}\sigma_{\theta\theta}^{(1)} + \sigma_{zz}^{(1)}\sigma_{\theta\theta}^{(1)}\right) + 2(1+\nu_1)\tau_{rz}^{(1)2}\Big\}\, r\, dr\; dz \tag{31}$$

$$\Pi_2 = \frac{\pi}{E_2} \int_0^L \int_c^d \left\{ \sigma_{rr}^{(2)2} + \sigma_{zz}^{(2)2} + \sigma_{\theta\theta}^{(2)2} - 2\nu_2 \left(\sigma_{rr}^{(2)} \sigma_{zz}^{(2)} + \sigma_{rr}^{(2)} \sigma_{\theta\theta}^{(2)} + \sigma_{zz}^{(2)} \sigma_{\theta\theta}^{(2)} \right) + 2(1+\nu_2) \tau_{rz}^{(2)2} \right\} r \, dr \, dz \tag{32}$$

$$\Pi_3 = \pi \int_0^L \int_b^c \frac{1}{E(z)} \left\{ \sigma_{rr}^{(a)2} + \sigma_{\theta\theta}^{(a)2} - 2\nu \sigma_{rr}^{(a)} \sigma_{\theta\theta}^{(a)} + 2(1+\nu) \tau_{rz}^{(a)2} \right\} r \, dr \, dz \tag{33}$$

Introducing expressions for stresses ($\sigma_{rr}^{(1)}$, $\sigma_{\theta\theta}^{(1)}$ and $\tau_{rz}^{(1)}$) in eqn. 31 and integrating the resulting expression over the radius r, the energy functional Π_1 reduces to

$$\Pi_1 = \pi \int_0^L \left(\bar{A}_1 + \bar{A}_2 \, \sigma_{zz}^{(1)} + \bar{A}_3 \, \frac{d^2 \sigma_{zz}^{(1)}}{dz^2} + A_{10} \, \sigma_{zz}^{(1)} \frac{d^2 \sigma_{zz}^{(1)}}{dz^2} + A_4 \left(\frac{d^2 \sigma_{zz}^{(1)}}{dz^2} \right)^2 + A_{11} \left(\frac{d\sigma_{zz}^{(1)}}{dz} \right)^2 \right) \, dz \tag{34}$$

The explicit expressions for the constants (function of material and geometric parameters) $\bar{A}_1$, $\bar{A}_2$, $\bar{A}_3$, A_{10}, A_4 and A_{11} are detailed in the appendix-A. Similarly, plugging expressions for stresses ($\sigma_{rr}^{(2)}$, $\sigma_{zz}^{(2)}$, $\sigma_{\theta\theta}^{(2)}$ and $\tau_{rz}^{(2)}$) in eqn. 32 and integrating the resulting expression over the radius r, the energy functional Π_2 reduces to

$$\Pi_2 = \pi \int_0^L \left(\bar{C}_1 + \bar{C}_2 \, \sigma_{zz}^{(1)} + C_3 \, \sigma_{zz}^{(1)2} + \bar{C}_3 \, \frac{d^2 \sigma_{zz}^{(1)}}{dz^2} + C_6 \, \left(\frac{d^2 \sigma_{zz}^{(1)}}{dz^2} \right)^2 + C_{15} \, \sigma_{zz}^{(1)} \frac{d^2 \sigma_{zz}^{(1)}}{dz^2} + C_{16} \left(\frac{d\sigma_{zz}^{(1)}}{dz} \right)^2 \right) \, dz \tag{35}$$

The explicit expressions for the material and geometric parameters $\bar{C}_1$, $\bar{C}_2$, C_3, $\bar{C}_3$, C_6, C_{15} and C_{16} are detailed in the appendix-A.

Again introducing expressions for ($\sigma_{\theta\theta}^{(a)}$, $\sigma_{rr}^{(a)}$ and $\tau_{rz}^{(a)}$) in eqn. 33 and integrating the resulting expression over the radius r, the energy functional for an FMGB adhesive becomes

$$\Pi_3 = \pi \int_0^L \left(\bar{B}_1(z) + \bar{B}_2(z) \, \frac{d^2 \sigma_{zz}^{(1)}}{dz^2} + B_7(z) \left(\frac{d\sigma_{zz}^{(1)}}{dz} \right)^2 + B_3(z) \, \left(\frac{d^2 \sigma_{zz}^{(1)}}{dz^2} \right)^2 \right) \, dz \tag{36}$$

The parameters $\bar{B}_1(z)$, $\bar{B}_2(z)$, $B_7(z)$ and $B_3(z)$ vary along the bondline and the expressions for these variable parameters are given in the appendix-A. Now combining eqns. 34, 35 and 36, the complimentary energy in the whole assembly is given by

$$\Pi = \pi \int_0^L \left(\beta_1 \sigma_{zz}^{(1)2} + \beta_2(z) \left(\frac{d^2\sigma_{zz}^{(1)}}{dz^2} \right)^2 + \beta_3 \sigma_{zz}^{(1)} \frac{d^2\sigma_{zz}^{(1)}}{dz^2} + \beta_4(z) \left(\frac{d\sigma_{zz}^{(1)}}{dz} \right)^2 + (\beta_5 + \chi_1 h(z)) \right.$$
$$\left. \frac{d^2\sigma_{zz}^{(1)}}{dz^2} + (\beta_6 + \chi_1 k)\, \sigma_{zz}^{(1)} + \left(\beta_7 + \chi_1^2 m(z) + \chi_1 s \right) \right) dz \tag{37}$$

In the above functional, the constant coefficients β_1, β_3, β_5, β_6, β_7, k, s and the variable coefficients $\beta_2(z)$, $\beta_4(z)$, $h(z)$ and $m(z)$ depend on geometrical and material properties and the loading conditions of the bonded joint and are given in the appendix-A.

The optimal value of χ_1 is given by

$$\pi \int_0^L \left(h(z)\ \frac{d^2\sigma_{zz}^{(1)}}{dz^2} + k\ \sigma_{zz}^{(1)} + 2\chi_1\ m(z) + s \right)\ dz \ = \ 0 \tag{38}$$

The above functional given by eqn. 37 can be expressed as function of φ

$$\Pi = \int_0^L \varphi \left(\sigma_{zz}^{(1)}, \frac{d\sigma_{zz}^{(1)}}{dz}, \frac{d^2\sigma_{zz}^{(1)}}{dz^2}, z \right) dz \tag{39}$$

We now need the differential equation satisfied by the function $\sigma_{zz}^{(1)}$ which minimizes the above functional. Performing variational calculus on the above functional yields

$$\frac{\partial\varphi}{\partial\sigma_{zz}^{(1)}} - \frac{d}{dz}\left(\frac{\partial\varphi}{\partial\sigma'_{zz}{}^{(1)}} \right) + \frac{d^2}{dz^2}\left(\frac{\partial\varphi}{\partial\sigma''_{zz}{}^{(1)}} \right) \ = \ 0 \tag{40}$$

where, $\sigma''_{zz}{}^{(1)} = \frac{d^2\sigma_{zz}^{(1)}}{dz^2}$, $\sigma'_{zz}{}^{(1)} = \frac{d\sigma_{zz}^{(1)}}{dz}$. Manipulating the above equation results in the following nonlinear fourth order ordinary differential equation.

$$\beta_2(z)\frac{d^4\sigma_{zz}^{(1)}}{dz^4} + 2\beta_2'(z)\frac{d^3\sigma_{zz}^{(1)}}{dz^3} + (\beta_3 - \beta_4(z) + \beta_2''(z))\frac{d^2\sigma_{zz}^{(1)}}{dz^2}$$
$$-\beta_4'(z)\frac{d\sigma_{zz}^{(1)}}{dz} + \beta_1\sigma_{zz}^{(1)} + \frac{\chi_1}{2}h''(z) + \frac{\beta_6 + \chi_1 k}{2} = 0 \tag{41}$$

The integral eqn. 38 and the differential eqn. 41 are to be solved simultaneously to find the actual $\sigma_{zz}^{(1)}$ and its derivatives to predict the stresses in the bonded system using the traction boundary conditions given by eqns. 19 and 20. The solution procedure is described in the appendix-A. We refer this model hereafter by the name 'FMGB1'.

5.2 Case II: FMGB ($\sigma_{rr}^{(i)} = 0, i.e \quad \chi_1 \to 0$)

If we neglect the radial stress in the assembly, i.e $\sigma_{rr}^{(i)} = 0$, the constant $\chi_1 \to 0$. Setting $\chi_1 = 0$ in the functional, Π given by eqn. 37 and performing variational calculus of the resulting functional, we recover the nonlinear differential equation of the model presented by Kumar [49] and is given below.

$$\beta_2(z)\frac{d^4\sigma_{zz}^{(1)}}{dz^4} + 2\beta_2'(z)\frac{d^3\sigma_{zz}^{(1)}}{dz^3} + (\beta_3 - \beta_4(z) + \beta_2''(z))\frac{d^2\sigma_{zz}^{(1)}}{dz^2} - \beta_4'(z)\frac{d\sigma_{zz}^{(1)}}{dz} + \beta_1\sigma_{zz}^{(1)} + \frac{\beta_6}{2} = 0 \tag{42}$$

In this model we have only a single fourth order differential equation with four traction boundary conditions given by eqns. 19 and 20 and it is numerically solved in Matlab using bvp4c program. The solution $\sigma_{zz}^{(1)}$ and its derivatives can be used to predict the stresses in the bonded system but noting that $\chi_1 = 0$. We refer this model hereafter by the name 'FMGB'.

5.3 Case III: MMB1 ($\sigma_{rr}^{(i)} \neq 0, i.e \quad \chi_1 \neq 0$)

When we have a mono modulus bondline (MMB) adhesive, the modulus function of the adhesive becomes a constant, $E(z) \to E$ and all the parameters of the model which are function of the bondlengh z become constant, i.e $\beta_2(z) \to \beta_2$, $\beta_4(z) \to \beta_4$, $h(z) \to h$ and $m(z) \to m$. Accordingly the complementary energy functional of the system, Π reduces to the following

$$\Pi = \pi \int_0^L \left(\beta_1\sigma_{zz}^{(1)2} + \beta_2 \left(\frac{d^2\sigma_{zz}^{(1)}}{dz^2}\right)^2 + \beta_3\, \sigma_{zz}^{(1)}\frac{d^2\sigma_{zz}^{(1)}}{dz^2} + \beta_4 \left(\frac{d\sigma_{zz}^{(1)}}{dz}\right)^2 + (\beta_5 + \chi_1\, h)\, \frac{d^2\sigma_{zz}^{(1)}}{dz^2} + (\beta_6 + \chi_1\, k)\, \sigma_{zz}^{(1)} + \left(\beta_7 + \chi_1^2\, m + \chi_1\, s\right) \right) dz \tag{43}$$

In this case, the optimal value of χ_1 is obtained by differntiating eqn. 43 with respect to χ_1 and equating the resulting expression to zero. The optimal value

of χ_1 is given by the following integral equation

$$\pi \int_0^L \left(h \ \frac{d^2\sigma_{zz}^{(1)}}{dz^2} + k \ \sigma_{zz}^{(1)} + 2\chi_1 \ m + s \right) \ dz \ = \ 0 \tag{44}$$

We now need the differential equation satisfied by the function $\sigma_{zz}^{(1)}$ which minimises the above functional given by eqn. 43. Performing variational calculus on this functional yields

$$\beta_2 \frac{d^4\sigma_{zz}^{(1)}}{dz^4} + (\beta_3 - \beta_4) \ \frac{d^2\sigma_{zz}^{(1)}}{dz^2} + \beta_1 \sigma_{zz}^{(1)} + \frac{\beta_6 + \chi_1 k}{2} = 0 \tag{45}$$

Now the fourth order linear ODE given by eqn. 45 and the integral equation given by eqn. 44 are simultaneously solved in Matlab using bvp4c program and using the boundary conditions given by eqns. 19 and 20. The solution procedure is same as that of the case I which is detailed in the appendix-A. Henceforth we refer this model by the name 'MMB1'.

5.4 Case IV: MMB ($\sigma_{rr}^{(i)} = 0, i.e \quad \chi_1 \to 0$)

When we have a mono modulus bondline (MMB) adhesive, the modulus function of the adhesive becomes a constant, $E(z) \to E$ and all the parameters of the model which are function of the bondlengh z become constant, i.e $\beta_2(z) \to \beta_2$ and $\beta_4(z) \to \beta_4$. Omission of radial stresses i.e $\sigma_{rr}^{(i)} = 0$ makes $\chi_1 = 0$. Accordingly the complementary energy functional of the system, Π given by eqn. 43 reduces to the following

$$\begin{aligned} \Pi = \pi \int_0^L \Bigg(& \beta_1 \sigma_{zz}^{(1)2} + \beta_2 \ \left(\frac{d^2\sigma_{zz}^{(1)}}{dz^2} \right)^2 + \beta_3 \ \sigma_{zz}^{(1)} \frac{d^2\sigma_{zz}^{(1)}}{dz^2} + \beta_4 \ \left(\frac{d\sigma_{zz}^{(1)}}{dz} \right)^2 \\ & + \beta_5 \ \frac{d^2\sigma_{zz}^{(1)}}{dz^2} + \beta_6 \ \sigma_{zz}^{(1)} + \beta_7 \Bigg) \ dz \end{aligned} \tag{46}$$

Performing variational calculus on the above functional yields the following fourth order linear ODE.

$$\beta_2 \frac{d^4\sigma_{zz}^{(1)}}{dz^4} + (\beta_3 - \beta_4) \ \frac{d^2\sigma_{zz}^{(1)}}{dz^2} + \beta_1 \sigma_{zz}^{(1)} + \frac{\beta_6}{2} = 0 \tag{47}$$

This ODE is solved in Matlab using bvp4c program and using the boundary conditions given by eqns. 19 and 20. Henceforth we refer this model by the

Table 1
Geometric and material properties of adhesive and adherends

Item	Material	E [GPa]	ν	a [mm]	b [mm]	c [mm]	d [mm]	f [MPa]
Tube 1	AU 4G	75	0.3	44.8	47.8	-	-	-
Tube 2	G0969/M18	44.080	0.325	-	-	48	50	100
Adhesive	AV119	2.7	0.35	-	47.8	48	-	-

name 'MMB'.

6 Properties of adherends and adhesives

The elastic properties of adherends and MMB adheives are given in Table 1.

7 Results and discussion

Initially, analysis of the joint under axial tensile was performed using FMGB1 model in which $\sigma_{rr}^{(i)} \neq 0$, considering isotopic adherends whose geometrical and mechanical properties are given in table 1 with a graded adhesive of modulus function E_{f_1} (E_m=2700 MPa, E_o=280 MPa and L=80 mm). Analysis was also performed using FMGB model in which $\sigma_{rr}^{(i)} = 0$, considering the same geometric, material and loading condition as those of FMGB1 model. The results were then compared to study the influence of non-zero radial stresses $\sigma_{rr}^{(i)}$ on peak shear and peel stresses and their distribution. Figs. 6 and 7 show the shear stress distribution in the members of the joint over the bondlegth using FMGB1 and FMGB models at their midplanes respectively. From these figures, we can see that the shear stress in the graded adhesive changes whereas the shear stresses in the adherends do not change appreciably. Fig. 8 shows the shear stress distribution at the midplane of the adhesive layer based on these two functionally graded models and also based on their respective mono modulus counterparts (i.e MMB1 model in which $\sigma_{rr}^{(i)} \neq 0$ and MMB model in which $\sigma_{rr}^{(i)} = 0$). The mono modulus adhesive properties are given in the table 1). Inclusion of radial stress components in the functionally graded model changes the shear stress peaks in the adhesive (8.7% in this case) and its distribution over the bond length appreciably and so does the mono modulus model. It can also be seen from Fig. 8 that shear stress peaks and its distribution in the adhesive layer predicted by the graded models are less severe than those of mono modulus models. The shear peak reduces by 19% by employing FMGB1 model in lieu of MMB1 model whereas it reduces by 17% by employing FMGB model in lieu of MMB model.

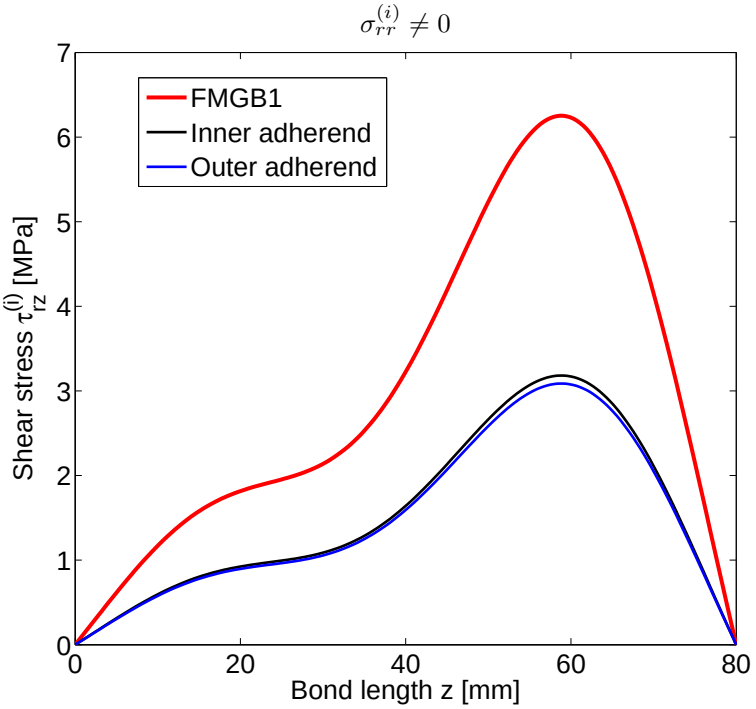

Fig. 6. Shear stress distribution at the midplanes of the adhesive layer, inner adherend and outer adherend using FMGB1 model in which $\sigma_{rr}^{(i)} \neq 0$

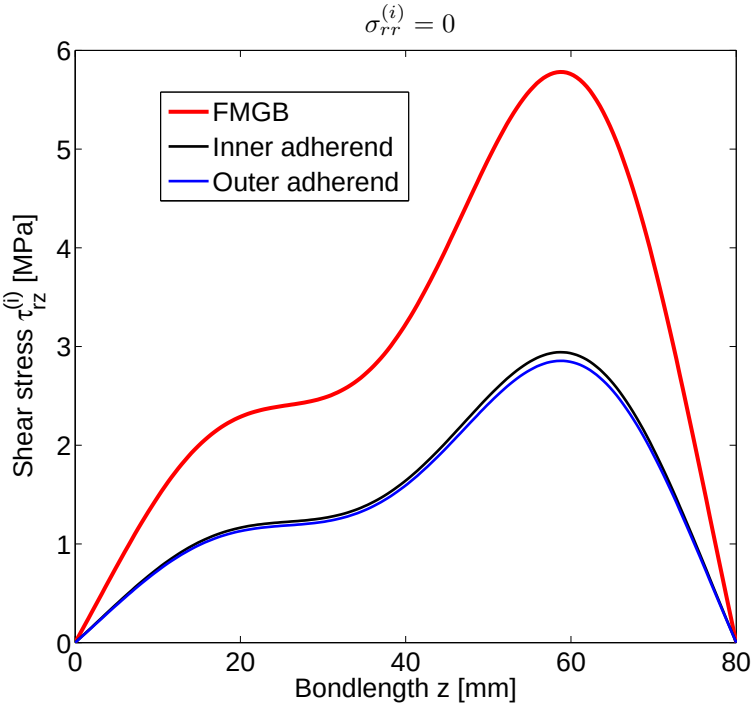

Fig. 7. Shear stress distribution at the midplanes of the adhesive layer, inner adherend and outer adherend using FMGB model in which $\sigma_{rr}^{(i)} = 0$

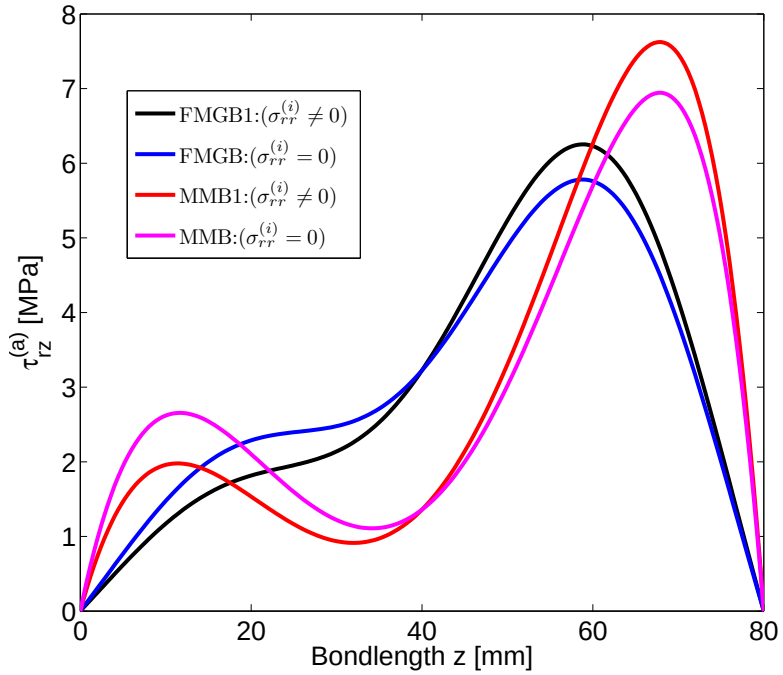

Fig. 8. Shear stress distribution at the midplane of adhesive layer based on graded and mono modulus models

Figs. 9 and 10 show the peel stress distribution in the members of the joint over the bondlength using FMGB1 and FMGB models at their midplanes respectively. From these figures, we can see that the peel stresses both in the graded adhesive and in the adherends change significantly unlike the shear shear stresses. Peak peel stress in the adhesive layer increases by 19% whereas peak peel stresses in the inner adherend and outer adherend increase by 150% and 180% respectively. Inclusion of radial stress components in the functionally graded model changes the peel stress peaks in the adhesive and adherends and its distribution over the bond length appreciably and so does the mono modulus model. Fig. 11 shows the peel stress distribution at the midplane of the adhesive layer based on these two functionally graded models and also based on their respective mono modulus counterparts (i.e MMB1 model in which $\sigma_{rr}^{(i)} \neq 0$ and MMB model in which $\sigma_{rr}^{(i)} = 0$). Drastic increase in peel stresses in the adhesive may lead to cohesive failure within the adhesive whereas the higher peel stresses in the adherends will lead to adhesive failure within adherends if composite adherends used have low through thickness transverse strength. It can also be seen from Fig. 11 that peel stress peaks and its distribution in the adhesive layer predicted by the graded models are less severe than those of mono modulus models. The peel peak stress reduces by 73% by employing FMGB1 model in lieu of MMB1 model whereas it reduces by 70% by employing FMGB model in lieu of MMB model. The shear and peel stress intensities both at interface and as well as at the midplane of adhesive

predicted by FMGB1 model are much smaller and their distribution along the bondline is more uniform than those of a MMB1 adhesive joint.

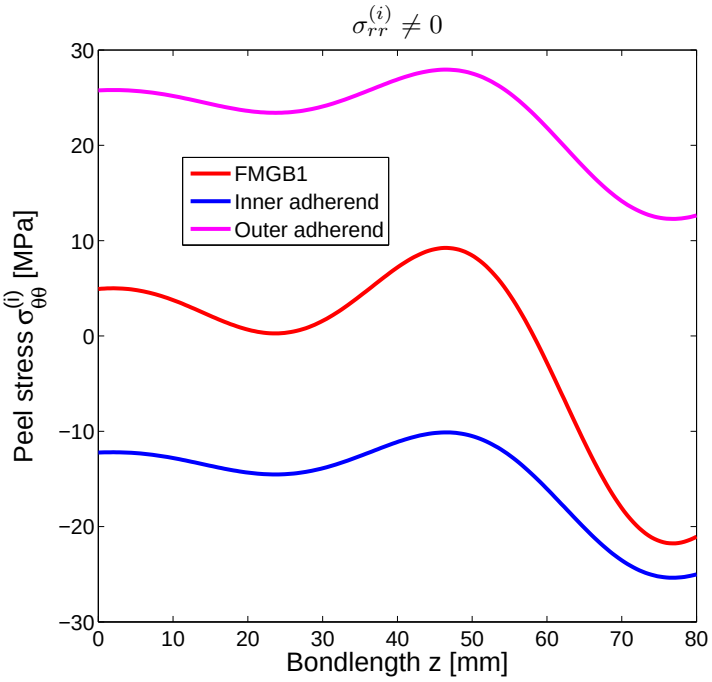

Fig. 9. Peel stress distribution at the midplanes of the adhesive layer, inner adherend and outer adherend using FMGB1 model in which $\sigma_{rr}^{(i)} \neq 0$

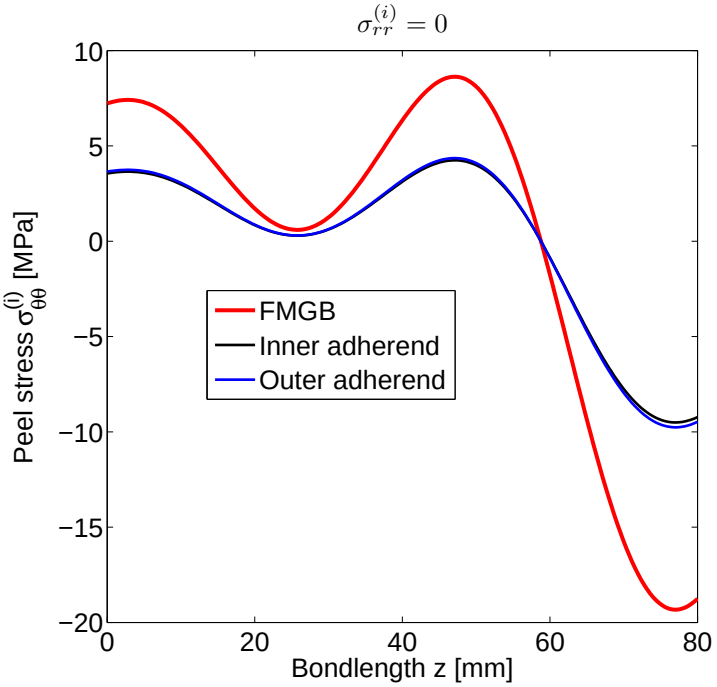

Fig. 10. Peel stress distribution at the midplanes of the adhesive layer, inner adherend and outer adherend using FMGB model in which $\sigma_{rr}^{(i)} = 0$

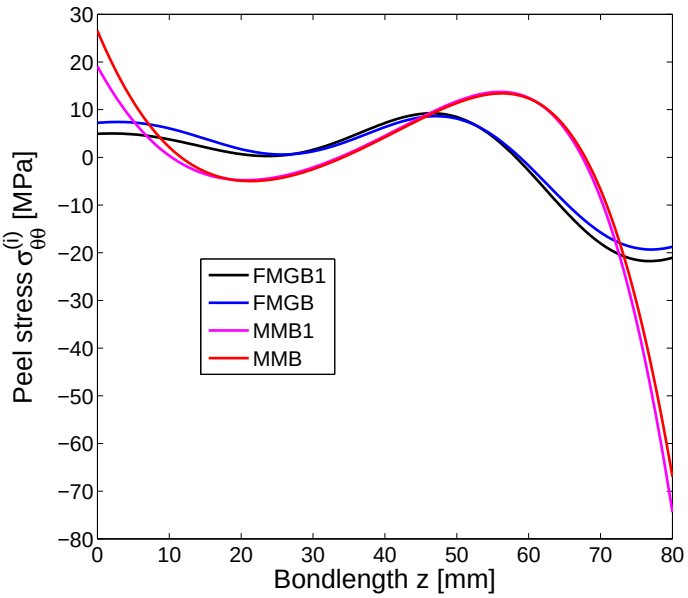

Fig. 11. stress distribution at the midplane of adhesive layer based on graded and mono modulus models

The peak peel stress in the FMGB adhesive joints appear close to the overlap ends, while it appears exactly at the overlap ends in a MMB adhesive joints. This is because the stiffness jump in FMGB joints is more gradual than in MMB joints.

7.1 Influence of bondlength (L)

Stress analyses have been carried out by varying the bondlength from 40 to 250 mm, and adopting the exponential modulus function profile E_{f1} for the adhesive using FMGB1 model in order to study the effect of bondlength on stress distribution. The prediction using FMGB1 model is also compared with the predictions of MMB1 model. Figs. 12 and 13 show the shear stress distribution at the midplane of the adhesive for selected values of bondlength.

At small bondlengths, the shear stress distribution in both FMGB1 and MMB1 adhesives are parabolic, with stress peaks at mid-bondlength. For $L \leq 50mm$, the shear stress in the graded adhesive is much severe than that of the mono modulus adhesive. Shear stress peaks predicted by both FMGB1 and MMB1 models decrease and their distribution becomes more uniform with increase of bondlength. Shear stress peak in the adhesive of the MMB1 model decreases with increase of bondlength from $L = 50mm$ upto $L = 80mm$ and increases for $L > 80mm$ but upto $L = 150mm$. Beyond a certain bondlength ($L = 150mm$),

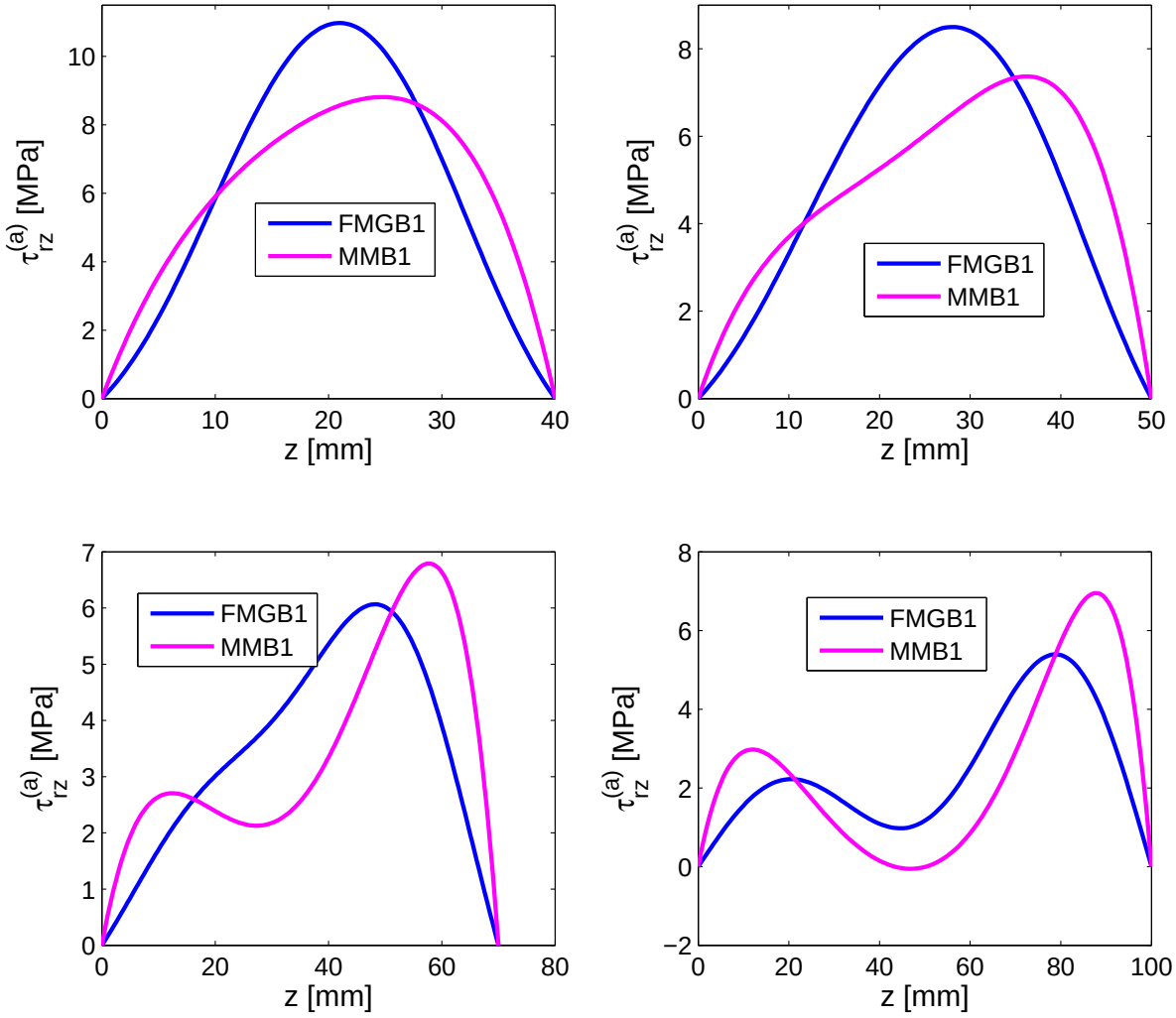

Fig. 12. Shear stress distribution at the midplane of the adhesive using FMGB1 model compared with that of MMB1 model as a function of bondlength

the increase of bondlength does not reduce the shear stress peak in the MMB1 adhesive appreciably. On the other hand, the peak shear stress in the FMGB1 adhesive decreases with increase of bondlength upto $L = 250mm$. In both models the shear stress peaks move close to overlap ends with increase of bondlength.

Figs. 14 and 15 show the peel stress distribution at the midplane of the adhesive for selected values of bondlength based on both FMGB1 and MMB1 models. For any value of bondlength peel stress peak in the graded bondline adhesive is much less and its distribution is more uniform than those of mono modulus bondline adhesive. An increase of bondlength reduces the peel stress

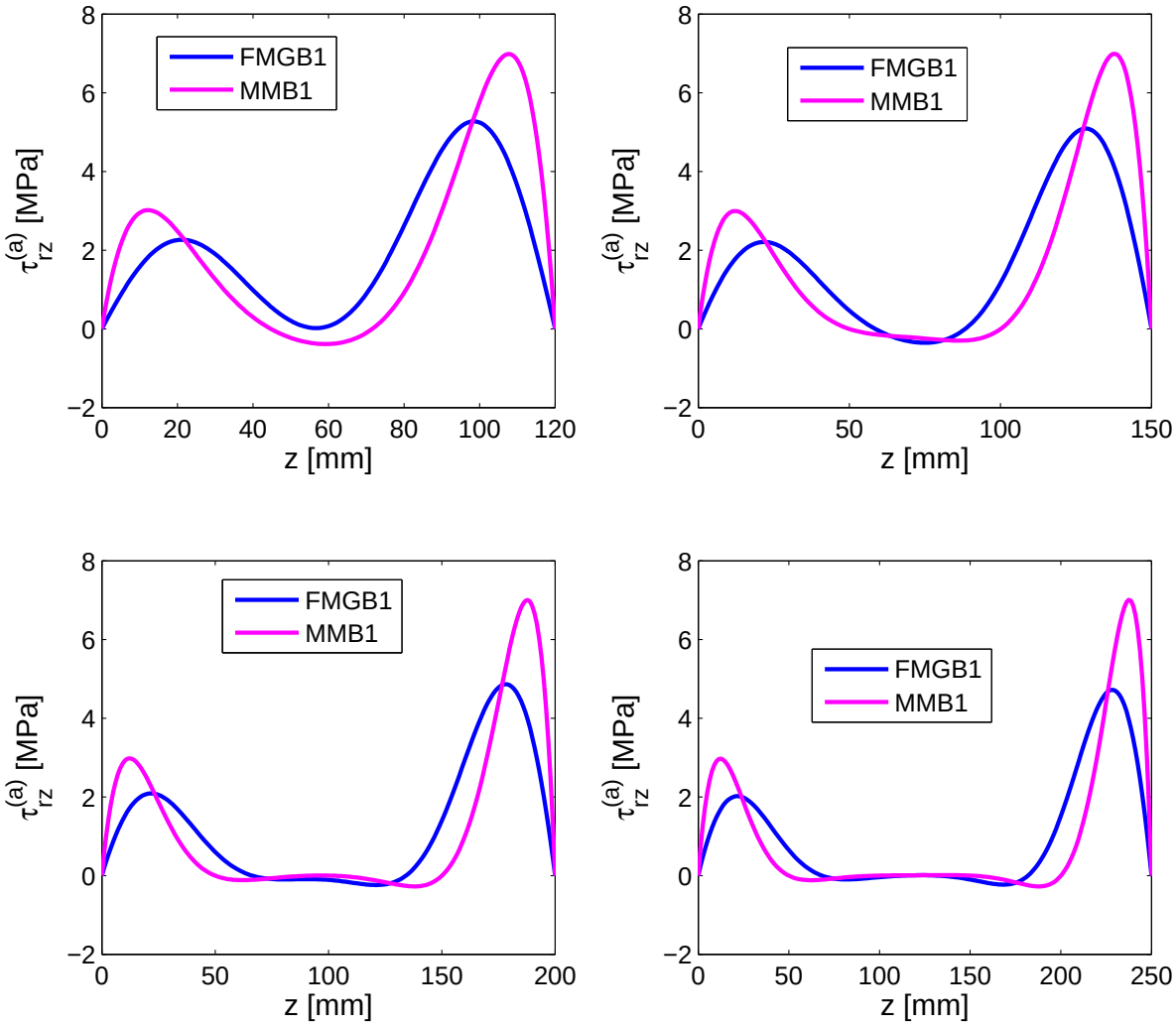

Fig. 13. Shear stress distribution at the midplane of the adhesive using FMGB1 model compared with that of MMB1 model as a function of bondlength

peak upto a certain bondlength ($L = 100mm$) and increases thereafter in FMGB1 adhesive whereas the shear stress peak in the MMB1 adhesive decreases upto $L = 80mm$ and increases with further increase of bondlength upto $L = 120mm$ and remains constant thereafter. Therefore, the bondlength at which the peel stress starts to increase with increase of bondlength is considered to be an optimum bondlength. The optimum bondlength in this case for FMGB1 model is is L=100mm. Both shear stress and peel stress peaks move towards the overlap ends with an increase of bondlength. However, the stress distribution does not change in the MMB1 joint after L=120 mm, for the variables used here.

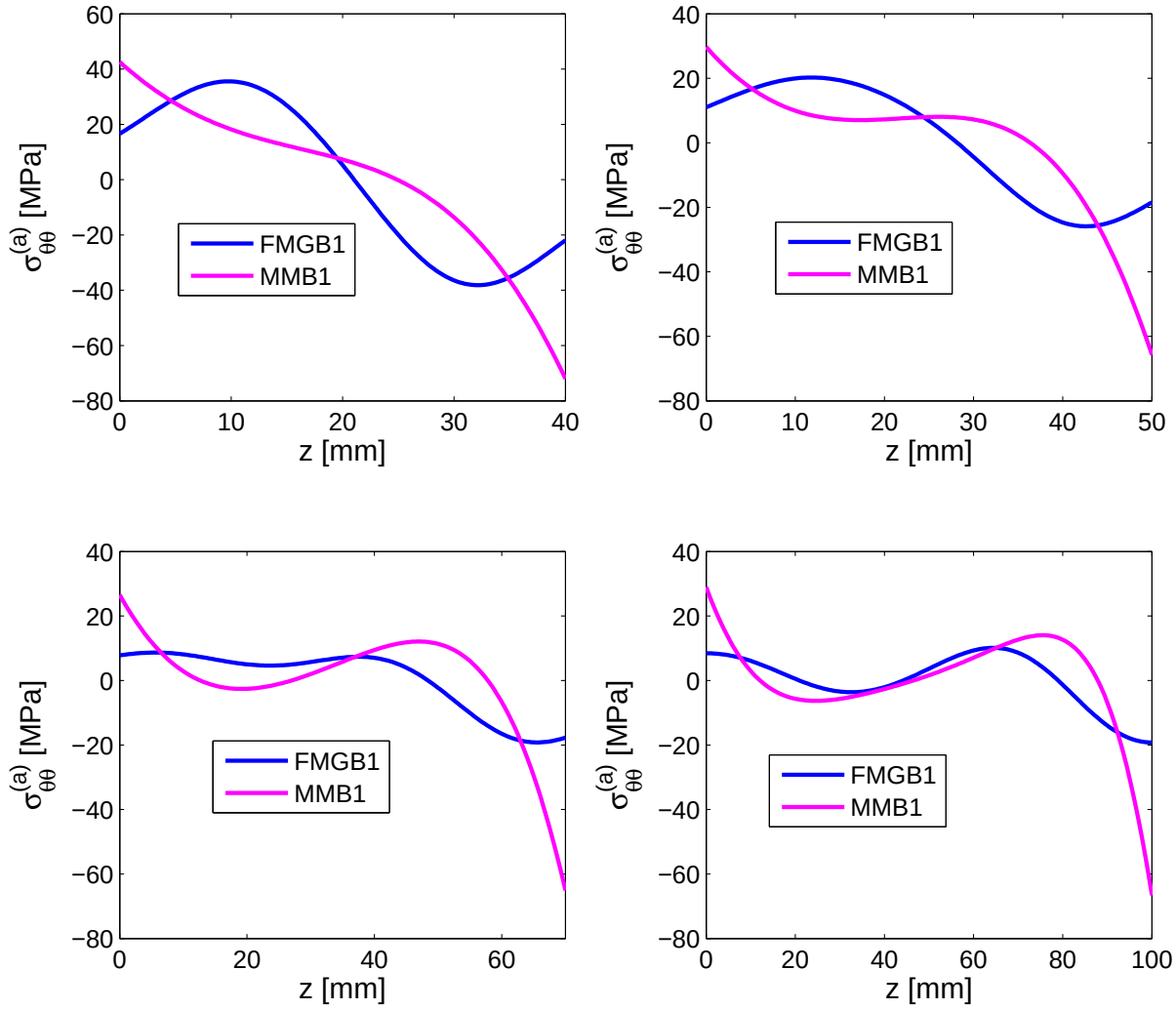

Fig. 14. Peel stress distribution at the midplane of the adhesive using FMGB1 model compared with that of MMB1 model as a function of bondlength

7.2 Influence of modulus function

Different modulus function profiles have been examined to reduce the stress peaks and gradients in the FMGB1 adhesive and also compared with adhesive stresses of MMB1 model. The shear and peel stress distributions for different modulus functions are shown in fig. 16 and fig. 17 respectively.

The shear stress intensity is less for modulus function E_{f3} while the peel stress intensity is less for modulus function E_{f2}. If we choose a stiff MMB1 adhesive to have maximum shear strength, it will fail due to high peel stresses. Unlike the MMB1 adhesive, the modulus function of the FMGB1 adhesive can be so

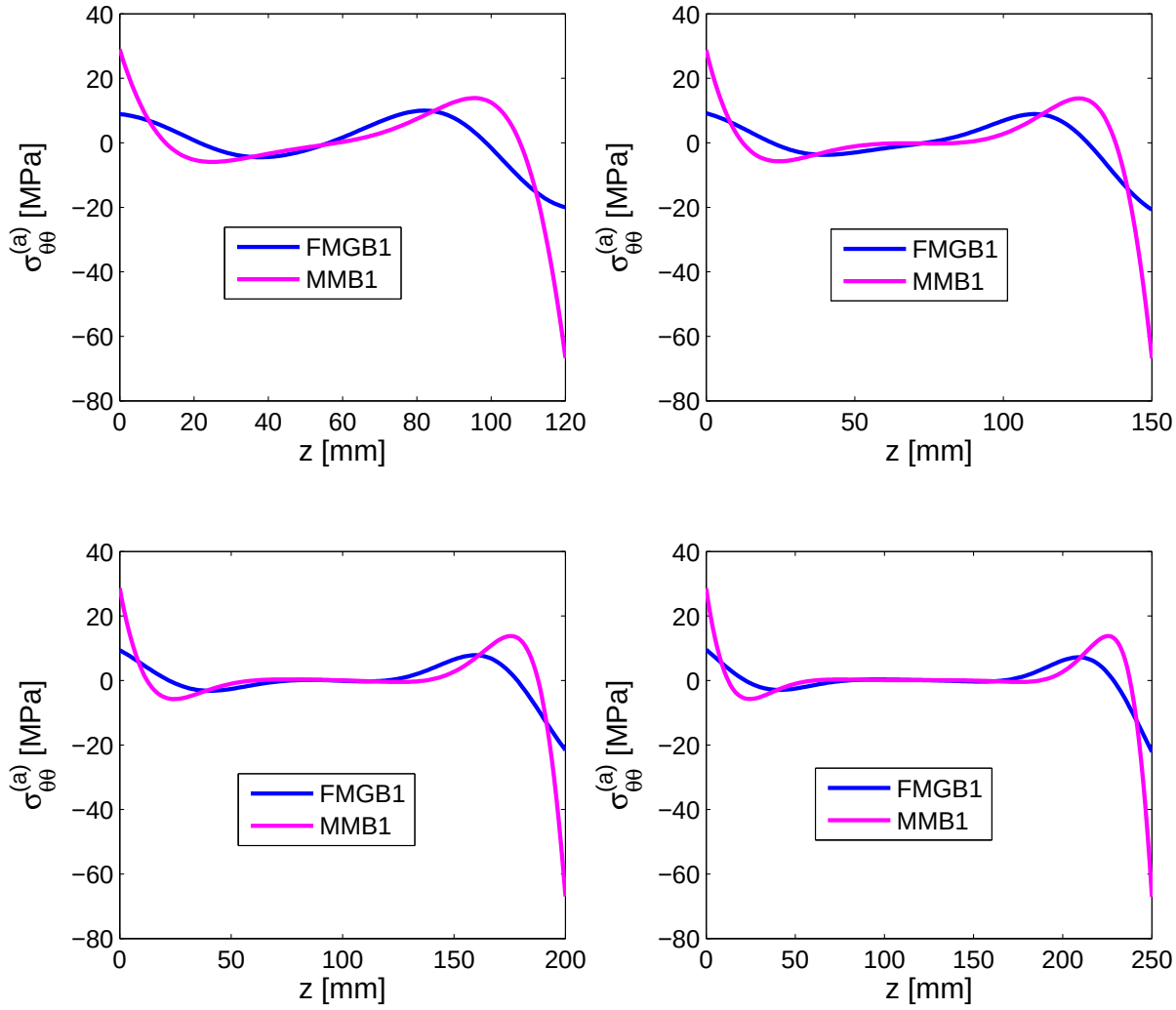

Fig. 15. Peel stress distribution at the midplane of the adhesive using FMGB1 model compared with that of MMB1 model as a function of bondlength

tailored simultaneously to achieve both shear and peel strengths.

7.3 Influence of stiffness mismatch

Note that for the balanced joint, the shear stress distribution is symmetric and the peel stress distribution is anti-symmetric about the mid bondlength. Deviation from the symmetric distribution of shear stress and anti-symmetric distribution of peel stress arises due to the axial stiffness mismatch between the two adherends.

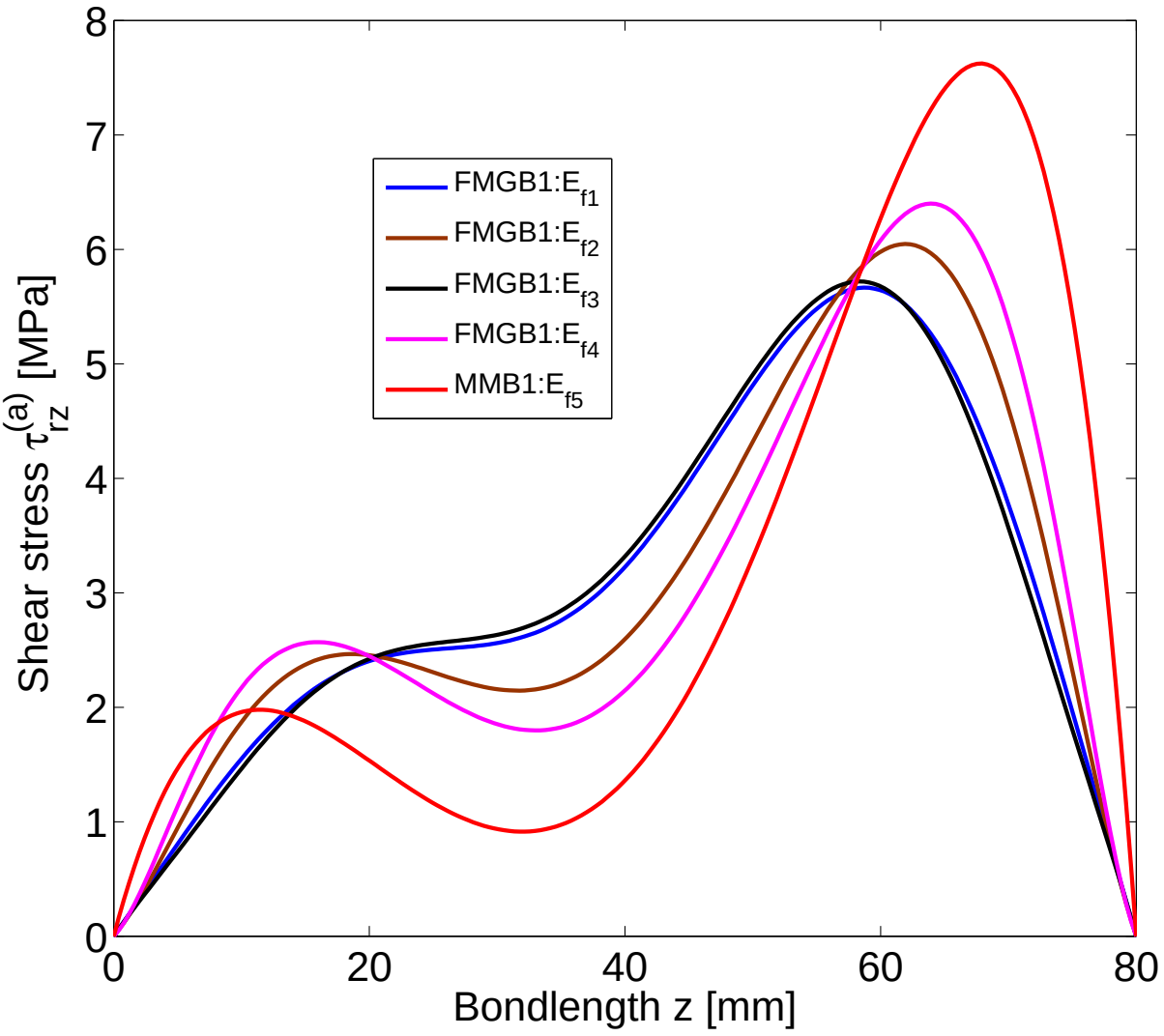

Fig. 16. Shear stress distribution at the midplane of the adhesive based on FMGB1 for different modulus functions

Figs. 18 and 19 show the shear and peel stress distribution at the midplane of the adhesive as a function of stiffness mismatch between two adherends. Note that the shear stress distribution looses its symmetry and peel stress distribution looses its anti-symmetry about mid-bondlength when $E_1A_1 \neq E_2A_2$. Here A_1 and A_2 are the area of cross section of inner and outer adherends respectively. The stress distribution is compared with the MMB1 adhesive and found that the stress distribution in FMGB1 adhesive is much less than MMB1 adhesive.

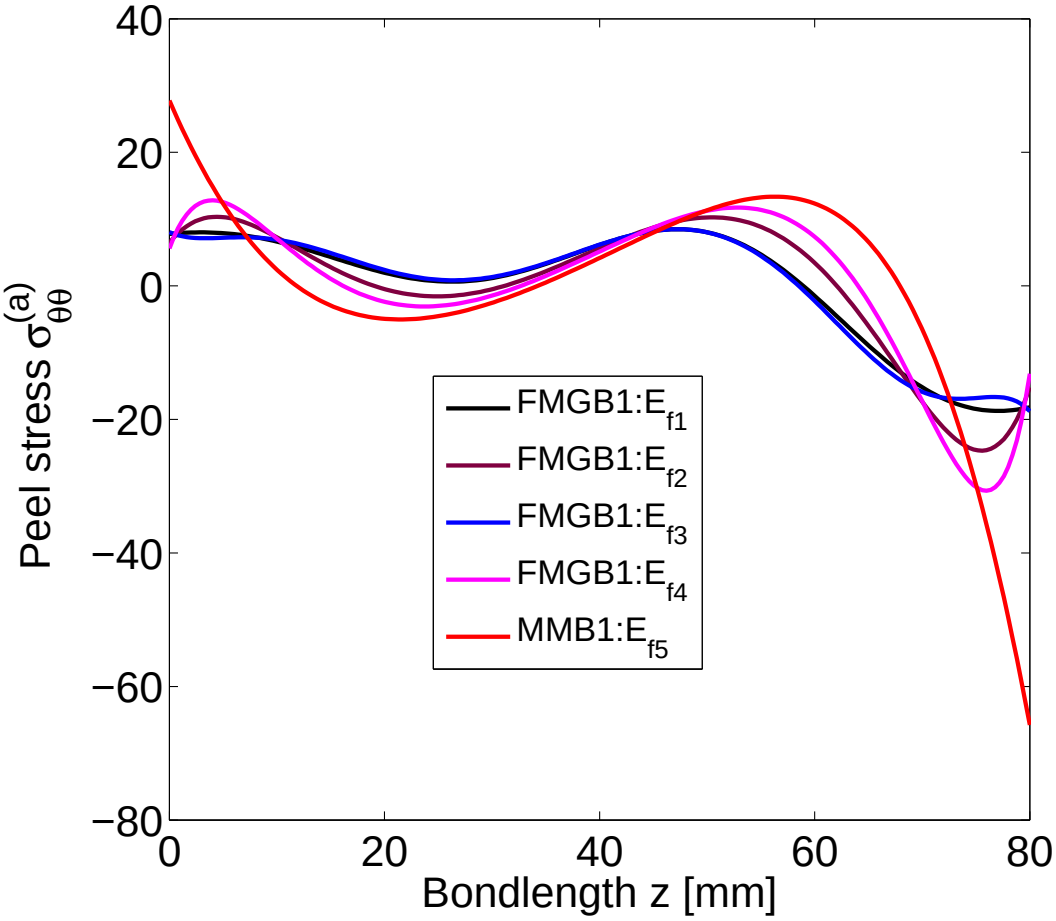

Fig. 17. Peel stress distribution at the midplane of the adhesive based on FMGB1 for different modulus functions

8 Conclusions

A fuller analytical model has been developed to study the stresses intensity and their distribution in a FMGB adhesive joint (FMGB1 model) based on a variational method, which minimizes the complimentary energy of the bonded system. It has been observed that the inclusion of radial stresses significantly influences the intensity and distribution of stresses in the joint. This refined model more accurately predicts the stresses not only in the adhesive but also in the adherends. It has been observed that the shear and peel stress concentrations at the overlap ends in the FMGB1 adhesive joints are much less than those of MMB1 adhesive joints under the same axial load. Reduced shear and peel stress concentrations provide improved joint strength and lifetime. Analysis also indicated that an optimized joint performance can be achieved by grading the modulus of the bondline adhesive. It has been observed through parametric evaluation that shear and peel stress peaks and its gradients in the

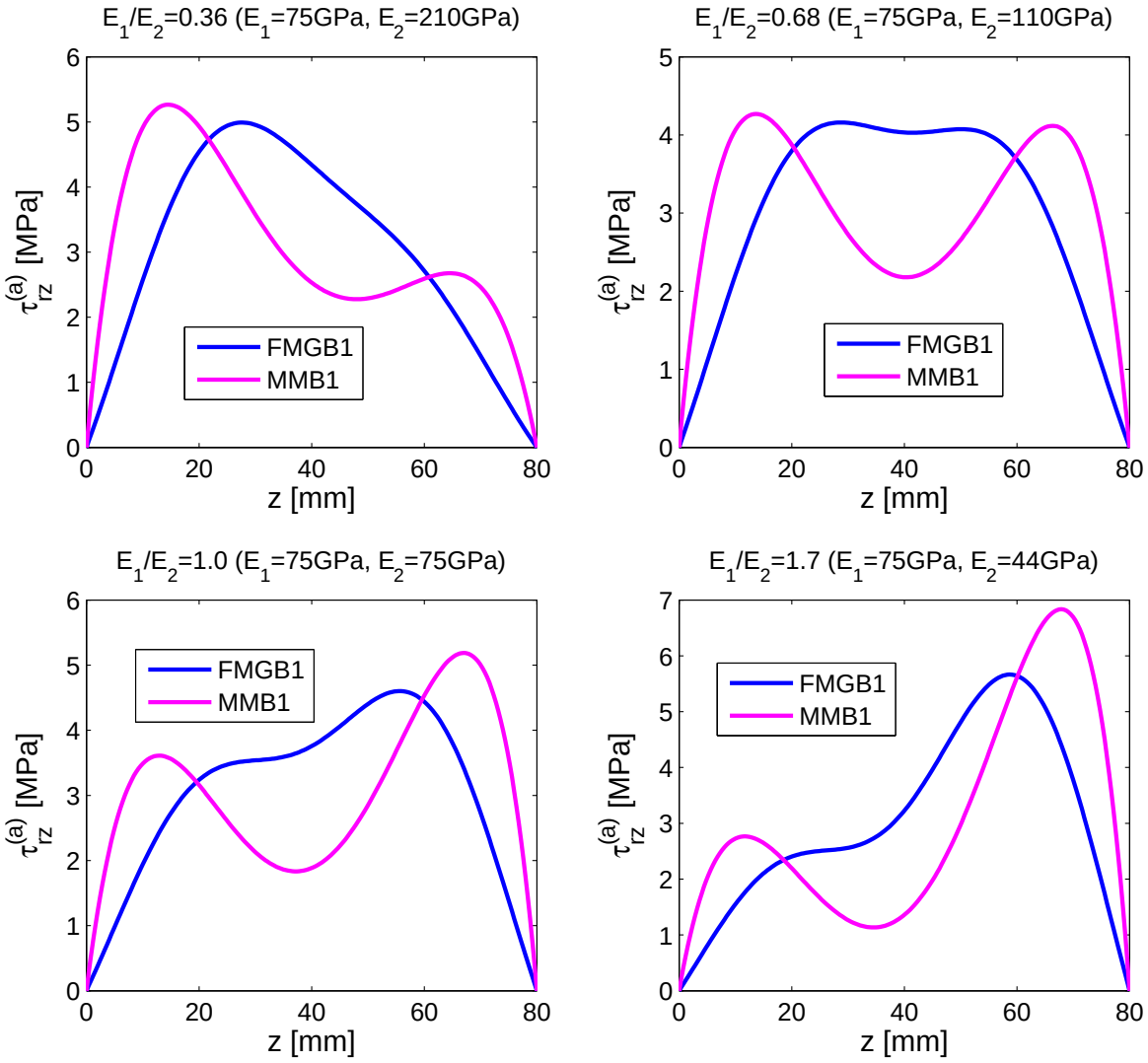

Fig. 18. Shear stress distribution at the midplane of the adhesive as a function of stiffness mismatch

bondline can be significantly reduced by selectively perturbing the geometrical and material properties of the bonded system.

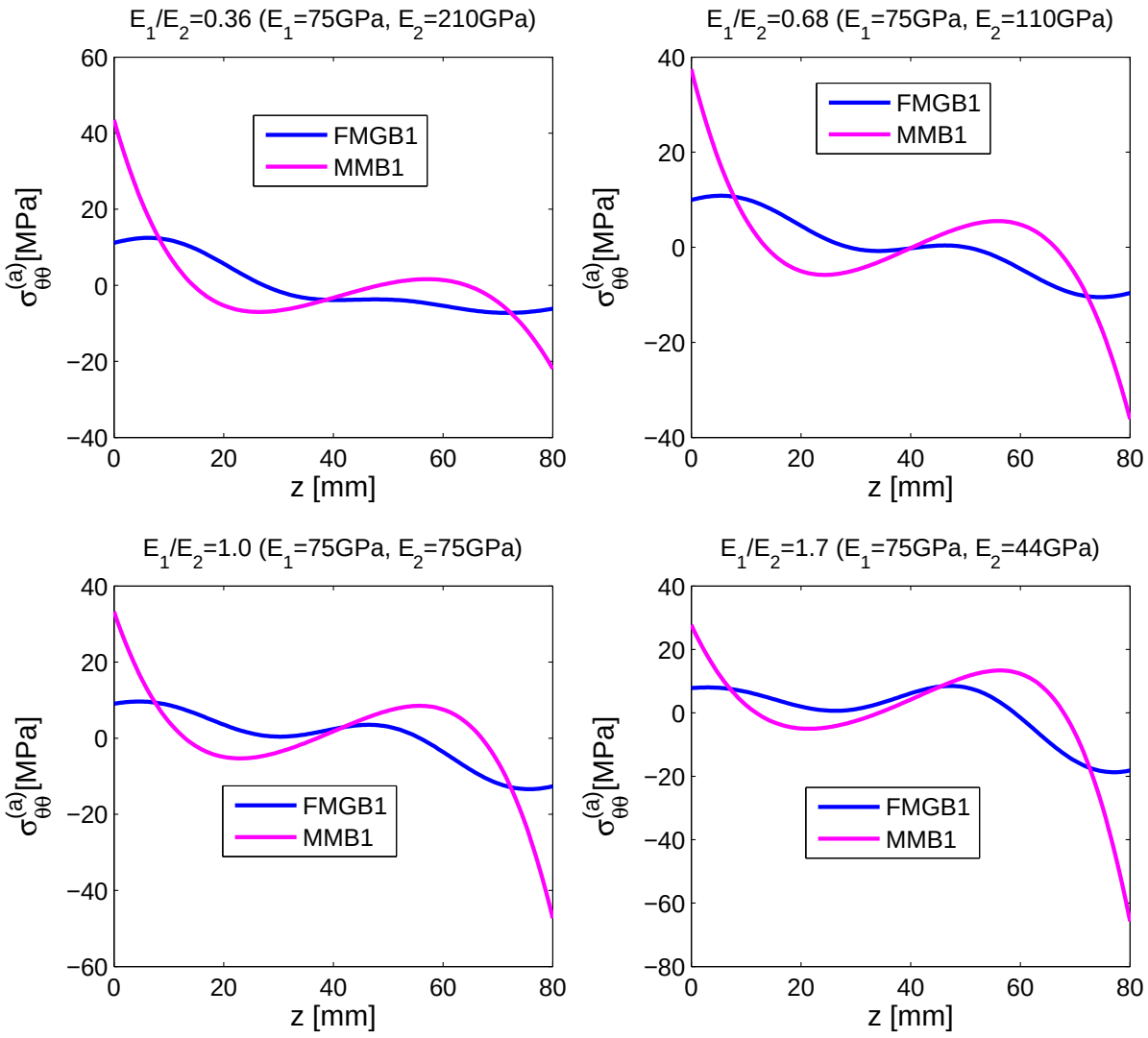

Fig. 19. Peel stress distribution at the midplane of adhesive as a function of stiffness mismatch

A Case I: FMGB1 ($\sigma_{rr}^{(i)} \neq 0, i.e \quad \chi_1 \neq 0$)

A.1 Inner adherend

The complimentary energy in the inner adherend is given by

$$\Pi_1 = \pi \int_0^L \left(\bar{A}_1 + \bar{A}_2 \ \sigma_{zz}^{(1)} + \bar{A}_3 \ \frac{d^2\sigma_{zz}^{(1)}}{dz^2} + A_{10} \ \sigma_{zz}^{(1)} \frac{d^2\sigma_{zz}^{(1)}}{dz^2} + A_4 \left(\frac{d^2\sigma_{zz}^{(1)}}{dz^2} \right)^2 + A_{11} \left(\frac{d\sigma_{zz}^{(1)}}{dz} \right)^2 \right) \ dz \tag{A.1}$$

The explicit expressions for the constants (function of material and geometric properties and loading condition of the joint) $\bar{A}_1$, $\bar{A}_2$, $\bar{A}_3$, A_{10}, A_4 and A_{11} are given below.

$$\xi_1 = 1/6\, b^6 - 1/6\, a^6 - 1/2\, a^2 \left(b^4 - a^4\right) + 1/2\, a^4 \left(b^2 - a^2\right) \ ; \quad A_1 = \frac{\chi_1^2}{E_1} \xi_1 \ ; \tag{A.2}$$

$$\xi_2 = 1/2\, \frac{b^2 - a^2}{E_1} \ ; \quad A_2 = \xi_2 \ ; \tag{A.3}$$

$$\xi_3 = 3/2\, b^6 - 3/2\, a^6 - 3/2\, a^2 \left(b^4 - a^4\right) + 1/2\, a^4 \left(b^2 - a^2\right) \ ; \quad A_3 = \frac{\chi_1^2}{E_1} \xi_3 \ ; \tag{A.4}$$

$$\xi_4 = 1/6\, b^6 - 1/6\, a^6 - 1/2\, a^2 \left(b^4 - a^4\right) + 1/2\, a^4 \left(b^2 - a^2\right) \ ; \quad A_4 = \frac{1}{4E_1} \xi_4 \ ; \tag{A.5}$$

$$\xi_5 = -1/2\, b^6 + 1/2\, a^6 + a^2 \left(b^4 - a^4\right) - 1/2\, a^4 \left(b^2 - a^2\right) \ ; \quad A_5 = \frac{\chi_1}{E_1} \xi_5 \ ; \tag{A.6}$$

$$\xi_6 = -1/4\, b^4 + 1/4\, a^4 + 1/2\, a^2 \left(b^2 - a^2\right) \ ; \quad A_6 = \frac{-2\nu_1\chi_1}{E_1} \xi_6 \ ; \tag{A.7}$$

$$\xi_7 = 1/2\, b^6 - 1/2\, a^6 - a^2 \left(b^4 - a^4\right) + 1/2\, a^4 \left(b^2 - a^2\right) \ ; \quad A_7 = \frac{-2\nu_1\chi_1^2}{E_1} \xi_7 \ ; \tag{A.8}$$

$$\xi_8 = -1/6\, b^6 + 1/6\, a^6 + 1/2\, a^2 \left(b^4 - a^4\right) - 1/2\, a^4 \left(b^2 - a^2\right) \ ; \quad A_8 = \frac{-\nu_1\chi_1}{E_1} \xi_8 \ ; \tag{A.9}$$

$$\xi_9 = -3/4\, b^4 + 3/4\, a^4 + 1/2\, a^2 \left(b^2 - a^2\right) \ ; \quad A_9 = \frac{-2\nu_1\chi_1}{E_1} \xi_9 \ ; \tag{A.10}$$

$$\xi_{10} = 1/4\, b^4 - 1/4\, a^4 - 1/2\, a^2 \left(b^2 - a^2\right) \ ; \quad A_{10} = \frac{-\nu_1}{E_1} \xi_{10} \ ; \tag{A.11}$$

$$\xi_{11} = 3/4\, a^4 - a^4 \ln(a) + 1/4\, b^4 - b^2 a^2 + a^4 \ln(b) \;\; ; \quad A_{11} = \frac{(1+\nu_1)}{2E_1}\xi_{11} \;\; ; \text{(A.12)}$$

$$\bar{A}_1 = A_1 + A_3 + A_7 \; ; \quad \bar{A}_2 = A_6 + A_9 \; ; \qquad \bar{A}_3 = A_5 + A_8 \; ; \qquad \text{(A.13)}$$

A.2 Outer adherend

The complimentary energy in the outer adherend is given by

$$\Pi_2 = \pi \int_0^L \left(\bar{C}_1 + \bar{C}_2\ \sigma_{zz}^{(1)} + C_3\ \sigma_{zz}^{(1)2} + \bar{C}_3\ \frac{d^2\sigma_{zz}^{(1)}}{dz^2} + C_6\ \left(\frac{d^2\sigma_{zz}^{(1)}}{dz^2}\right)^2 \right.$$
$$\left. + C_{15}\ \sigma_{zz}^{(1)} \frac{d^2\sigma_{zz}^{(1)}}{dz^2} + C_{16} \left(\frac{d\sigma_{zz}^{(1)}}{dz}\right)^2 \right)\ dz \qquad \text{(A.14)}$$

The explicit expressions for the constants $\bar{C}_1$, $\bar{C}_2$, C_3, $\bar{C}_3$, C_6, C_{15} and C_{16} are given below.

$$\eta_1 = 1/6\, d^6 - 1/6\, c^6 - 1/2\, d^2 \left(d^4 - c^4\right) + 1/2\, d^4 \left(d^2 - c^2\right) \;\; ; \quad C_1 = \chi_1^2 \frac{\rho^2}{E_2}\eta_1 \; ; \text{(A.15)}$$

$$C_2 = 1/2\, \frac{f^2\,(d^2 - c^2)}{E_2} \; ; \qquad \text{(A.16)}$$

$$C_3 = 1/2\, \frac{\rho^2\,(d^2 - c^2)}{E_2} \;\; ; \qquad \text{(A.17)}$$

$$C_4 = \frac{f\rho\ (d^2 - c^2)}{E_2} \;\; ; \qquad \text{(A.18)}$$

$$\eta_2 = 3/2\, d^6 - 3/2\, c^6 - 3/2\, d^2 \left(d^4 - c^4\right) + 1/2\, d^4 \left(d^2 - c^2\right) \;\; ; \quad C_5 = \chi_1^2 \frac{\rho^2}{E_2}\eta_2 \; ; \text{(A.19)}$$

$$\eta_3 = 1/6\, d^6 - 1/6\, c^6 - 1/2\, d^2 \left(d^4 - c^4\right) + 1/2\, d^4 \left(d^2 - c^2\right) \;\; ; \quad C_6 = \frac{\rho^2}{4E_2}\eta_3 \; ; \text{(A.20)}$$

$$\eta_4 = -1/2\, d^6 + 1/2\, c^6 + d^2 \left(d^4 - c^4\right) - 1/2\, d^4 \left(d^2 - c^2\right) \;\; ; \quad C_7 = \chi_1 \frac{\rho^2}{E_2}\eta_4 \; ; \text{(A.21)}$$

$$\eta_5 = -1/4\, d^4 + 1/4\, c^4 + 1/2\, d^2 \left(d^2 - c^2\right) \;\; ; \quad C_8 = -2\nu_2\chi_1\ \rho\frac{f}{E_2}\eta_5 \; ; \text{(A.22)}$$

$$C_9 = -2\nu_2\chi_1\ \frac{\rho^2}{E_2}\eta_5 \; ; \qquad \text{(A.23)}$$

$$\eta_6 = 1/2\, d^6 - 1/2\, c^6 - d^2\left(d^4 - c^4\right) + 1/2\, d^4\left(d^2 - c^2\right)\ ; \quad C_{10} = -2\nu_2\chi_1^2\ \frac{\rho^2}{E_2}\eta_6\ ; \text{(A.24)}$$

$$\eta_7 = -1/6\, d^6 + 1/6\, c^6 + 1/2\, d^2\left(d^4 - c^4\right) - 1/2\, d^4\left(d^2 - c^2\right)\ ; \quad C_{11} = -\nu_2\chi_1\ \frac{\rho^2}{E_2}\eta_7\ ; \text{(A.25)}$$

$$\eta_8 = -3/4\, d^4 + 3/4\, c^4 + 1/2\, d^2\left(d^2 - c^2\right)\ ; \quad C_{12} = -2\nu_2\chi_1\ f\frac{\rho}{E_2}\eta_8\ ; \text{(A.26)}$$

$$C_{13} = -2\nu_2\chi_1\ \frac{\rho^2}{E_2}\eta_8\ ; \tag{A.27}$$

$$\eta_9 = 1/4\, d^4 - 1/4\, c^4 - 1/2\, d^2\left(d^2 - c^2\right)\ ; \quad C_{14} = -\nu_2\ f\frac{\rho}{E_2}\eta_9\ ; \tag{A.28}$$

$$C_{15} = -\nu_2\ \frac{\rho^2}{E_2}\eta_9\ ; \tag{A.29}$$

$$\eta_{10} = -1/4\, c^4 + c^2 d^2 - d^4 \ln(c) - 3/4\, d^4 + d^4 \ln(d)\ ; \quad C_{16} = (1+\nu_2)\ \frac{\rho^2}{2E_2}\eta_{10}\ ; \text{(A.30)}$$

$$\bar{C}_1 = C_1 + C_2 + C_5 + C_8 + C_{10} + C_{12}\ ; \quad \bar{C}_2 = C_4 + C_9 + C_{13}\ ; \quad \bar{C}_3 = C_7 + C_{11} + C_{14}\ ; \tag{A.31}$$

A.3 FMGB adhesive

The complementary energy functional for an FMGB adhesive is given by

$$\Pi_3 = \pi \int_0^L \left(\bar{B}_1(z) + \bar{B}_2(z)\ \frac{d^2\sigma_{zz}^{(1)}}{dz^2} + B_7(z)\left(\frac{d\sigma_{zz}^{(1)}}{dz}\right)^2 + B_3(z)\ \left(\frac{d^2\sigma_{zz}^{(1)}}{dz^2}\right)^2 \right)\ dz \text{(A.32)}$$

The parameters $\bar{B}_1(z)$, $\bar{B}_2(z)$, $B_7(z)$ and $B_3(z)$ vary along the bondline and the expressions for these variable parameters are given below.

$$\lambda_1 = \left(a^2 - b^2\right)^2\left(c^2 - b^2\right)\ ; \quad B_1(z) = \chi_1^2\ \frac{1}{2E(z)}\lambda_1\ ; \tag{A.33}$$

$$\lambda_2 = \lambda_1\ ; \quad B_2(z) = B_1(z)\quad ; \tag{A.34}$$

$$\lambda_3(z) = 1/8\ \frac{\left(b^2 - a^2\right)^2\left(c^2 - b^2\right)}{E(z)}\ ; \quad B_3(z) = \lambda_3(z)\ ; \tag{A.35}$$

$$\lambda_4 = \left(a^2 - b^2\right)\left(b^2 - a^2\right)\left(c^2 - b^2\right)\ ; \quad B_4(z) = \frac{\chi_1}{2E(z)}\lambda_4\ ; \tag{A.36}$$

$$\lambda_5 = \lambda_2\ ; \quad B_5(z) = -\nu\frac{\chi_1^2}{E(z)}\lambda_5\ ; \tag{A.37}$$

$$\lambda_6 = \lambda_4 \; ; \qquad B_6(z) = -\nu \frac{\chi_1}{2E(z)} \lambda_6 \; ; \tag{A.38}$$

$$\lambda_7 = 1/4 \left(b^2 - a^2\right)^2 \left(-\ln(b) + \ln(c)\right) \; ; \qquad B_7(z) = \frac{2(1+\nu)}{E(z)} \lambda_7 \; ; \tag{A.39}$$

$$\bar{B}_1(z) = B_1(z) + B_2(z) + B_5(z) \; ; \quad \bar{B}_2(z) = B_4(z) + B_6(z) \; ; \tag{A.40}$$

A.4 Complementary energy of the whole assembly

Now combining eqns. A.1, A.14 and A.32, the complimentary energy in the whole assembly is given by

$$\Pi = \pi \int_0^L \left(\beta_1 \sigma_{zz}^{(1)2} + \beta_2(z) \left(\frac{d^2 \sigma_{zz}^{(1)}}{dz^2} \right)^2 + \beta_3 \sigma_{zz}^{(1)} \frac{d^2 \sigma_{zz}^{(1)}}{dz^2} + \beta_4(z) \left(\frac{d\sigma_{zz}^{(1)}}{dz} \right)^2 + (\beta_5 + \chi_1 h(z)) \right.$$
$$\left. \frac{d^2 \sigma_{zz}^{(1)}}{dz^2} + (\beta_6 + \chi_1 k) \sigma_{zz}^{(1)} + \left(\beta_7 + \chi_1^2 m(z) + \chi_1 s \right) \right) dz \tag{A.41}$$

In the above functional, the constant coefficients β_1, β_3, β_5, β_6, β_7, k, s and the variable coefficients $\beta_2(z)$, $\beta_4(z)$, $h(z)$ and $m(z)$ depend on geometrical and material properties and the loading conditions of the bonded joint and are given below.

$$\beta_1 = A_2 + C_3 \; ; \quad \beta_2(z) = A_4 + B_3(z) + C_6 \; ; \quad \beta_3 = A_{10} + C_{15} \; ; \tag{A.42}$$

$$\beta_4(z) = A_{11} + B_7(z) + C_{16} \; ; \quad \beta_5 = C_{14} \; ; \quad \beta_6 = C_4 \; ; \quad \beta_7 = C_2 \; ; \tag{A.43}$$

$$k = -2 \left[\frac{\nu_1}{E_1} (\xi_6 + \xi_9) + \frac{\nu_1}{E_1} \rho^2 (\eta_5 + \eta_8) \right] \; ; \tag{A.44}$$

$$s = -2\nu_2 \rho \, \frac{f}{E_2} (\eta_5 + \eta_8) \, ; \tag{A.45}$$

$$m(z) = \frac{\xi_1 + \xi_3 - 2\,\nu_1\,\xi_7}{E_1} + \frac{\lambda_1\,(1-\nu)}{E(z)} + \frac{\rho^2 (\eta_1 + \eta_2 - 2\,\nu_2\,\eta_6)}{E_2} \tag{A.46}$$

$$h(z) = \frac{\xi_5 - \nu_1\,\xi_8}{E_1} + 1/2\,\frac{\lambda_4\,(1-\nu)}{E(z)} + \frac{\rho^2 \left(\eta_4 - \nu_2\,\eta_7\right)}{E_2} \tag{A.47}$$

A.5 Solution procedure

Differentiating the functional given by eqn. A.41 with respect to χ_1 and setting that zero yields optimal value of χ_1 and is given by

$$\pi \int_0^L \left(h(z)\ \frac{d^2\sigma_{zz}^{(1)}}{dz^2} + k\ \sigma_{zz}^{(1)} + 2\chi_1\ m(z) + s \right)\ dz \ = \ 0 \tag{A.48}$$

Performing variational calculus of the functional (eqn. A.41) gives the following nonlinear fourth order ODE.

$$\begin{aligned} \beta_2(z)\frac{d^4\sigma_{zz}^{(1)}}{dz^4} + 2\beta_2'(z)\frac{d^3\sigma_{zz}^{(1)}}{dz^3} + (\beta_3 - \beta_4(z) + \beta_2''(z))\frac{d^2\sigma_{zz}^{(1)}}{dz^2} \\ -\beta_4'(z)\frac{d\sigma_{zz}^{(1)}}{dz} + \beta_1\sigma_{zz}^{(1)} + \frac{\chi_1}{2}h''(z) + \frac{\beta_6 + \chi_1 k}{2} = 0 \end{aligned} \tag{A.49}$$

The integral eqn. A.48 and the differential eqn. A.49 are simultaneously solved to get the solution $\sigma_{zz}^{(1)}$ in Matlab using bvp4c program with traction boundary conditions given by eqns. 19 and 20. Eqn. A.49 can be solved only if we know the value of χ_1. But χ_1 can be evaluated only if we know the stress function $\sigma_{zz}^{(1)}$. However, the crux of the problem is to determine the actual $\sigma_{zz}^{(1)}$ which minimises the complementary energy of the bonded system. Therefore, we initially find the approximate value of χ_1 by fitting a cubic polynomial for the stress function $\sigma_{zz}^{(1)}$ since we know four boundary conditions ($\sigma_{zz}^{(1)}$ and $\frac{d\sigma_{zz}^{(1)}}{dz}$) at the ends of the overlap. Then we use this approximate value of χ_1 together with traction BCs given by eqns. 19 and 20 to find the solution of the differential eqn. A.49. Now we have the numerical approximate solution of $\sigma_{zz}^{(1)}$ and its derivatives over the entire bondlength. Now we use this solution set to evaluate a new χ_1 solving the integral equation (eqn. A.48). Again use this current value of χ_1 to solve the DE. This process is repeated until the value of χ_1 attains a constant value i.e $\left(\chi_1^{(i+1)} - \chi_1^{(i)}\right) \approx 0$. This $\chi_1^{(i+1)}$ is the optimal value and the $\sigma_{zz}^{(1)}$ corresponding to this $\chi_1^{(i+1)}$ is the actual stress state. Once we know actual distribution of $\sigma_{zz}^{(1)}$ and its derivatives, we can get the complete stress state in the entire system.

References

[1] **Lubkin J L, Reissner E.** *Stress distribution and design data for adhesive lap joints between circular tubes*, **Journal of Applied Mechanics** 1958;78:1213-1221.

[2] **Volkersen O.** *Luftfahrtforschung* 1938;15:41-47.

[3] **Goland M, Reissner E.** *The stresses in cemented joints* , **Jl of Applied Mechanics, Trans ASME** 1944;66:A17-27.

[4] **Hart-Smith L J.** *An engineer's viewpoint on design and analysis of aircraft structural joints* , **Jl of Aerospace Eng G. IMechE** 1995.

[5] **Wooley G R, Carver.** *Stress concentration factors for bonded lap joints*, **J. Aircraft** 1971;8:817-820.

[6] **Adams R D, Peppiatt N A.** *Stress analysis of adhesively bonded lap joints*, **J. strain Anal.**1974;9:185-196.

[7] **Crocombe A D, Adams R D.** *Influence of spew fillet and other parameters on the stress distribution in the single-lap joint*, **J. Adhesion**1981;13:141-155.

[8] **Adams R D, Peppiatt N A.** *Stress analysis of adhesively bonded tubular lap joint*, **J. Adhesion** 1977;9(1):1-18.

[9] **Nagaraja Y R, Alwar R S.** *Viscoelastic analysis of an adhesive-bonded plane lap joint*, **Computers Structures**1980;11:621-627.

[10] **Harris, Adams R D.** *Strength prediction of bonded single lap joints by non-linear finite element methods*, **Int. J. Adhesion Adhesives**1984;4:65-78.

[11] **Pickett A K, Hollaway L.** *The analysis of elastic-plastic adhesive stress in bonded lap joints in FRP structures*, **Composite Structures**1985;4:135-160.

[12] **Oplinger.** *A layered beam theory for single lap joints*, **Army Materials Technology Laboratory Report**1991,MTL TR91-23.

[13] **Tsai M Y, Morton J.** *On analytical and numerical solutions to the single-lap joint*, **Center for Adhesive and Sealant Science**1993,VPI, Report CASS/ESM-92-8.

[14] **Deb A., et al.** *An experiemental and analytical study of mechanical behaviour of adhesively bonded joints for variable extension rates and temperatures*, **Int Journal of adhesion and adhesives**2007;28:1-15.

[15] **Allman D J.** *A theory for elastic stresses in adhesive bonded lap joints*, **Quart. J. Mech. Appl. Math.**1977;30:415-436.

[16] **Shi Y P, Cheng S.** *Analysis of adhesive-bonded cylindrical lap joints subjected to axial load*, **J. Eng. Mech**1993;119(3):584-602.

[17] **Lindon J., et al.** *Calculation of the strength of cylindrical assemblies with an anaerobic adhesive*, **J. Adhesion Sci. Techonol.,** 2005;19(1):41-56.

[18] **Pugno N, Carpinteri A.** *Tubular adhesive joints under axial load*, **Transactions of the ASME** 2003;70:832-839.

[19] **Imanaka M., et al.** *Fatigue life estimation of adhesive bonded shaft joints*, **Int. J. Fracture** 1989;41:223-234.

[20] **Nayeb-Hashemi H., et al.** *Multiaxial fatigue life evaluation of tubular adhesively bonded joints*,**Int. J. Adhesion and Adhesives** 1997;17:55-63.

[21] **Thomsen O T.** *Elasto-static and elasto-plastic stress analysis of adhesive bonded tubular lap joints*,**Composite Structures** 1992;21:249-259.

[22] **Kim Y G., et al.** *Strength of adhesively-bonded tubular single lap carbon/epoxy composite-steel joints*,**J. Composite Materials** 1999;33(20):1897-1917.

[23] **Nemes O., et al.** *Contribution to the study of cylindrical adhesive joining*, **Int. J. Adhesion and Adhesives** 2006;26:474-480.

[24] **Her S C.** *Stress analysis of adhesively bonded lap joints* , **Compos Struct** 1999;47:673-678.

[25] **Apalak M K.** *Geometrically nonlinear analysis of adhesively bonded corner joints* , **Jl of Adhes Sci Technol** 1999;13(11):A17-27.

[26] **Penado F E.** *Analysis of singular regions in bonded joints* , **Int Jl of Fract** 2000;105(1):1-25.

[27] **Erdogan F, Ratwani M.** *Stress distribution in bonded joints* , **Jl of Compos Mater** 1971;5:378-93.

[28] **Amijima S, Fujii T.** *Simple stress analysis method for adhesive bonded tapered joints* , **Int Journal of adhesion and adhesives** 1989;9(3):155-60.

[29] **Kim J S, Kim C G, Hong C S.** *Practical design of tapered composite structures using the manufacturing cost concept* , **Comps Struct** 2001;51(3):285-299.

[30] **Lang T P, Mallick P K.** *The effect of recessing on the stresses in adhesively bonded single-lap joints* , **Int Journal of adhesion and adhesives** 1999;19:257-271.

[31] **Lang T P, Mallick P K.** *The effect of spew geometry on adhesive stress distributions in laminated composite joints* , **Int Journal of adhesion and adhesives** 1998;18(3):167-177.

[32] **Tsai M Y, Morton J.** *The effect of a spew fillet geometry on stresses in single lap adhesive joints* , **Compos Struct**1995;32(1-4):123-131.

[33] **Krieger R B.** *Stress analysis concepts for adhesive bonding of aircraft primary structure* , **In: Adhesively Bonded Joints: Testing, Analysis, and Design, ASTM STP**1988;981:264-275.

[34] **Sadek M M.** *Industrial applications of adhesive bonding* , **Elsevier Applied Science Publishers**1987, UK.

[35] **Ganesh V K, Choo T S.** *Modulus graded composite adherends for single-lap bonded joints*, **J. Composite Materials** 2002;36(14):1757-1767.

[36] **Boss J N., et al. (2003)** *Modulus grading versus geometrical grading of composite adherends in single-lap bonded joints* , **Compos Struct**, Vol.62, pp.113-121.

[37] **Pires I., et al.** *Performance of bi-adhesive bonded aluminium lap joints* , **Int Journal of adhesion and adhesives** 2003;23:215-223.

[38] **Pires I., et al.** *Numerical simulation of mono- and bi-adhesive aluminium lap joints* , **J. Adhesion Sci. Techonol.,** 2006;20(1):19-36.

[39] **Fitton M D, Broughton J G.** *Variable modulus adhesive: an approach to optimised joint performance*, **Int Journal of adhesion and adhesives**2005;25:329-336.

[40] **Temiz S.** *Application of bi-adhesive in double-strap joints subjected to bending moment*, **J. Adhesion Sci. Techonol.,** 2006;20(14):1547-1560.

[41] **Kumar S, Pandey P C.** *Bi-adhesive bonded joints*, **J. Adhesion Sci. Technol.,** 2010;24(7):1251-1281.

[42] **Da Silva L F M, Adams R D.** *Adhesive joints at high and low temperatures using similar and dissimilar adherends and dual adhesives*, **Int Journal of adhesion and adhesives** 2007;27:216-227.

[43] **Chalkley P, Rose F.** *Stress analysis of double-strap bonded joints using a variational method*, **Int Journal of adhesion and adhesives** 2001;21:241-247.

[44] **Mengel R., et al.** *Mechanical properties of hub/shaft joints adhesively bonded and cured under hydrostatic pressure*, **Int Journal of adhesion and adhesives** 2007;27:568-573.

[45] **Pandey P C, Kumar S.** *Three dimensional non-linear finite element studies on adhesively bonded Crack-Patch Repairs*, **Aeronautical Development Board,ARDB Project No: DRAO/08/1051165/M/I** 2005.

[46] **Kumar S, Pandey P C.** *Cyclic-fatigue performance of adhesively bonded lap joint*, **Failure Mechanics Letters** 2005;1(1):4-5.

[47] **Pandey P C, Kumar S.** *Adhesively Bonded Patch-Repairs with Composites*, **Defence Science Journal** 2010;60(3):320-329.

[48] **Kumar S, Pandey P C.** *Fatigue life prediction of adhesively bonded single lap joints*, **Int Journal of adhesion and adhesives** 2011;31(1):43-47.

[49] **Kumar S.** *Analysis of Tubular Adhesive Joints with a Functionally Modulus Graded Bondline Subjected to Axial Loads*, **Int Journal of adhesion and adhesives** 2009;29:785-795.

[50] **Kumar S, Scanlan J. P.** *Stress Analysis of Shaft-Tube Bonded Joints Using a Variational Method*, **Journal of Adhesion** 2010;86(04):369-394.

[51] **Pandey P C., et al.** *Nonlinear analysis of adhesively bonded lap joints considering viscoplasticity in adhesives*, **Comp. Struc** 1999;70(4):387-413.

[52] **Pandey P C., et al.** *Three-dimensional nonlinear analysis of adhesively bonded lap joints considering viscoplasticity in adhesives*, **Comp. Struc** 2001;79(7):769-783.